AN ABSTRACT OF THE THESIS OF

Andreas Goebel for the degree of Master of Science in Physics presented on March 2, 1994.

Title: NMR Investigation of Cadmium Telluride Single Crystals Doped with Group III Elements

Redacted for Privacy

Abstract approved: _____

William W. Warren

Pulsed nuclear magnetic resonance (NMR) has been used in this study to probe the hyperfine interaction in cadmium telluride single crystals. The samples were undoped - as a reference sample - and doped with indium to concentrations of $1 \times 10^{19}\text{cm}^{-3}$ and $1.5 \times 10^{20}\text{cm}^{-3}$ and with gallium to a concentration of 10^{19}cm^{-3}. NMR measurements on the nuclei ^{115}In,^{69}Ga,^{71}Ga and ^{113}Cd were done. The doped samples show a substantial skin effect, which excluded the use of echo sequences and therefore a saturation sequence was used in almost all of the measurements.

No definite resonance was found for ^{115}In in the indium doped crystals.

Gallium resonances were found for both isotopes ^{69}Ga,^{71}Ga. By comparison of the respective spin-lattice relaxation times the dominating relaxation process in this sample was determined as being due to coupling of the nuclei to time dependent electric field gradients rather than due to coupling to conduction electrons. The number density of free carriers in this sample is $n = 2.5 \times 10^{15}\text{cm}^{-3}$ at $T = 330$ K. It is surprising to be able to detect gallium resonances since the amount of trapping of electrons is high and thus the number of defects must be considerable. Despite these

unfavorable circumstances three different environments of gallium were found. One part sits on lattice sites without static field gradients. Another fraction experiences a small field gradient with a coupling constant of about 3.5 kHz. A third fraction experiences a distribution of field gradients.

^{113}Cd was extensively studied. The spin-lattice relaxation time T_1 was measured in all crystals for temperatures between 210 K and 493 K. A temperature dependent chemical shift described by $\delta(T) = ((316 \pm 2) - (0.12 \pm 0.02)T)$ ppm with respect to a 0.1 molar $CdSO_4$ solution was found for this isotope. The ^{113}Cd nuclei in the undoped and in the gallium doped sample exhibit a single resonance line with a shift of (276 ± 2) ppm at 300 K and 280 ppm at 273 K respectively. The ^{113}Cd nuclei in the indium doped samples show up to five resonances with different spin-lattice relaxation times T_1. The splitting between the peaks is about 10 ppm and the peak which is shifted the furthest compared to the undoped sample has the highest relaxation rate. The fraction of nuclei showing the four additional and unexpected lines is about one percent. Therefore values for the relaxation rates couldn't be measured due to the small signal intensity. An explanation for the splitting in these five resonance lines is not yet known, but it seems to be connected to the use of indium as a donor. The only obvious difference between the gallium and indium doped samples being the higher carrier concentration of about $n = 3.5 \times 10^{17}\text{cm}^{-3}$ in the later case, which is a factor of 140 higher than in the gallium doped sample, the splitting may also be due to a higher number of free electrons.

NMR Investigation of Cadmium Telluride Single Crystals Doped with Group III Elements

by

Andreas Goebel

A THESIS

submitted to

Oregon State University

in partial fulfillment of
the requirements for the
degree of

Master of Science

Completed March 2, 1994
Commencement June 1994

Master of Science thesis of Andreas Goebel presented on March 2, 1994

APPROVED

Redacted for Privacy

Major Professor, representing Physics

Redacted for Privacy

Chair of Department of Physics

Redacted for Privacy

Dean of Graduate School

I understand that my thesis will become part of the permanent collection of Oregon State University libraries. My signature below authorizes release of my thesis to any reader upon request.

Redacted for Privacy

Andreas Goebel, Author

ACKNOWLEDGEMENT

It is not possible to thank all the special people I had the fortune to get to know and be inspired by during my time at Oregon State University. However, I would like to take the opportunity to recognize a few of them.

Foremost, I would like to thank my adviser, Dr. William W. Warren. Without his assistance, encouragement and moral support this work would not have been completed.

I wish to thank the members of the NMR group Christian Pilgrim, Show-Jye Cheng, Neil Roberts, Scott Fuller and Sue Klein for all the discussions and their suggestions.

The excellent layout of this document in LATEX wouldn't have been possible without the help of Jörg Schray.

A special thanks to my parents without their support and reassurance this journey to wisdom wouldn't have been possible.

The people, who made life in Corvallis enjoyable truly deserve recognition: Mitch and Barb, Peter, Jitka, Tom and Kara, Christian and Katrin, Mark, Lynn. I will miss the runs, the bike rides and "Let's go to Smith at the weekend". I am indebted to all of you.

I am especially thankful for the gift to get to know Mariani Omar. Her inspiration, spirit and sincerity never fail to encourage me.

TABLE OF CONTENTS

LIST OF FIGURES

LIST OF TABLES

NMR INVESTIGATION OF CADMIUM TELLURIDE SINGLE CRYSTALS DOPED WITH GROUP III ELEMENTS

1. INTRODUCTION

"Rather than strive for the ultimate purity it is important to understand the native defect problem and achieve a happy balance." K. Zanio [1, p.38]

Nuclear Magnetic Resonance (NMR) is a powerful technique to probe the local environment of nuclei on a microscopic scale and selectively for distinct isotopes and thus it can be used to study point defects. This is particularly interesting if point defects are associated or complexed with a certain nuclei of the sample, e.g. the dopant in a semiconductor. However, it is necessary, that the nuclei and the defects associated with them are in a high enough concentration in the material, since the signal amplitude is directly proportional to the number of spins under investigation. In the case of studies of dopants, which are usually 10^{14} to 10^{20} nuclei per cm^3, one is restricted to spins with a high natural abundance and to highly doped samples to get a minimum of roughly 10^{17} to 10^{18} nuclei per cm^3. The magnetic moment and the quadrupole moment of the species of interest are important, since they determine the signal strength and the width of the resonance line. The spin lattice relaxation mechanism is important, since it has to be fast enough to allow a high repetition rate of the signal acquisition process to make up for small signal intensities.

This work is concerned with NMR measurements on group III dopants in cadmium telluride, which is from the family of II-VI wide-bandgap semiconductor

compounds. Their bandgaps range from 3.2 – 1.44 eV. They are used in many applications today and they are candidates for many interesting devices like light-emitting diodes and laser diodes in the visible region. The difficulties in producing durable p-n-junctions in these materials is blamed on intrinsic point defects [2]. There are studies on point defects in these materials using Perturbed Angular Correlation (PAC) [2], [10], [9], [11] and their results suggest that one should be able to study complexes of the indium dopant and nearby vacancies using NMR.

1.1. PROPERTIES OF THE MATERIAL

1.1.1. Crystal Structure

Cadmium telluride (CdTe) single crystals at atmospheric pressure have the zinc blende structure, i.e. they consist of two interpenetrating face centered cubic sublattices offset from one another by one fourth of a body diagonal. One of these sublattices is occupied by cadmium atoms and one by tellurium atoms. The coordinates of the Te atoms being $000, 0\frac{1}{2}\frac{1}{2}, \frac{1}{2}0\frac{1}{2}, \frac{1}{2}\frac{1}{2}0$, the coordinates of the Cd atoms are found by adding $\frac{1}{4}$ of a lattice constant along each coordinate direction. This yields $\frac{1}{4}\frac{1}{4}\frac{1}{4}, \frac{1}{4}\frac{3}{4}\frac{3}{4}, \frac{3}{4}\frac{1}{4}\frac{3}{4}, \frac{3}{4}\frac{3}{4}\frac{1}{4}$ as coordinates of the Cd atoms. Every atom is tetrahedrally surrounded by four atoms of the other kind with an interatomic distance of $a\frac{\sqrt{3}}{4}$. The cubic lattice parameter a is the length of the side of a cubic cell of the face centered cubic sublattices and it is $a = 6.477\mathring{A}$ at room temperature.

1.1.2. General Properties

CdTe has a density of $\rho = 5.86$ gcm^{-3} at 300 K, its melting point is $T_{melt} = 1365$ K. Its minimum room temperature energy gap is $E_{gap} = 1.44$ eV

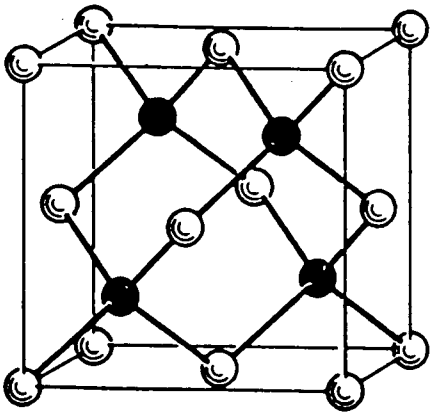

FIG. 1.1. Zinc Blende Structure

and it increases towards lower temperatures $E_{gap}(T = 80\ \mathrm{K}) = 1.60$ eV. It is a direct-gap semiconductor, i.e. the minimum of the conduction band and the maximum of the valence band are at $\overrightarrow{k} = 0$. The conduction band is formed from the first unoccupied levels of the cations, i.e. the 5s level of cadmium, whereas the uppermost valence band is made up from the highest occupied level of the anions, i.e. the 5p level of the tellurium atoms [3, p.56]. CdTe exhibits the highest ionicity of all II-VI compound semiconductors. Further data such as the effective masses of holes and electrons, dielectric constants and the refractive index can be found in table 2.11 of Hartmann, Mach, Selle [3].

1.1.3. Applications

CdTe is used in a vast variety of fields. It is used as a γ- and x-ray detector. Due to its large average atomic number $Z = 50$ the photoelectric effect, in which all of the photon energy is transferred to a tightly bound electron, is very effective. The wide band gap permits use of these detectors at temperatures up to 100° C.

CdTe is used as a solar cell, photoconductor, optical coating and in optical elements such as lenses, Brewster windows and partial reflectors.

CdTe alloyed with mercury ($Hg_{1-x}Cd_xTe$) is used as an infrared detector, since its bandgap can be varied continuously from $E_{gap} = -0.254$ eV to 1.6 eV as a function of alloy composition [4].

1.2. LITERATURE REVIEW

This is a short overview of the data on dopants and defects in cadmium telluride motivating this work.

1.2.1. Doping Properties

In all of the II-VI compounds shallow donors as well as shallow acceptors have been found, but for a group of them (ZnO, ZnSe, CdS, CdSe) it was not possible to make them p-type with a low resistivity nor to produce ZnTe as an n-type semiconductor. CdTe is very interesting since it can be produced as n-doped and as p-doped material with low resistivity. The energy levels of the dopants of interest here (group III elements) range between 0.011 eV−0.022 eV [5, table 11.4] below the top of the conduction band. Therefore aluminum, gallium and indium are shallow donors in CdTe substituting for cadmium in the lattice.

The solubility limit of indium in CdTe is very high. Over a temperature range 200° C−850° C concentrations between 10^{17} and 10^{21} atoms per cm^3, which were introduced by diffusion, have been observed [6].

The number of free carriers in indium doped CdTe varies strongly if one anneals the sample after it is grown. For example CdTe crystals grown with a dopant concentration of 1×10^{17} cm^{-3} of indium were highly resistive without any

temperature treatment. After annealing them at 2 atm of cadmium overpressure at $T = 900°$ C for 1.5h, 0.28×10^{17} cm^{-3} free carriers were found and after 24 h they increased to 1.6×10^{17} cm^{-3} [7].

For samples which were annealed in the same way, the number of free carriers depends strongly on the dopant concentration. Watson et. al. [6] found for indium doped samples that above a concentration of about 10^{16} cm^{-3} the number of free carriers increases more slowly than the dopant concentration and above 10^{19} dopant nuclei per cm^3 it actually decreases. Compensation effects can therefore be rather strong in this material.

The diffusion process of indium and gallium in CdTe seems to involve cadmium vacancies since the diffusion coefficient decreases with increasing cadmium partial pressure [8], [6].

1.2.2. Defect Complexes: Indium with a Cadmium Vacancy

A series of papers has been published on Perturbed Angular Correlation (PAC) measurements on indium doped CdTe [2], [10], [9], [11]. All of them show that indium sits in a variety of sites of different electric field gradients. The electric field gradients are believed to be caused by cadmium vacancies which have complexed with the indium dopants. The indium sites have been characterized and the results of the individual papers match each other. The number of individual sites strongly depends on the annealing procedures which have been applied.

The PAC measurements use radioactive ^{111}In as a probe nucleus, which decays into an excited ^{111}Cd nucleus subsequently undergoing a $\gamma-\gamma-$ cascade. The angular distribution of this cascade is perturbed by the electric field gradient at the site of the nucleus. Therefore their data on the quadrupole coupling constant involve

the quadrupole moment (Q~0.8 barns) of the ^{111}Cd excited state ($I = \frac{5}{2}, T_{1/2} = 85$ ns). This has to be taken into consideration to make predictions for the NMR results.

Although the numerical results of these publications are not identical, they show the same order of magnitude for a certain defect complex, i.e. they agree that a substantial fraction ($\sim$ 25%) of indium dopants are in a cubic site without an electric field gradient. Another fraction ($\sim 30 - 80\%$) of the probe nuclei sits in an electric field gradient which is almost axially symmetric with its main component along the $\langle 111 \rangle$ axis of the crystal. The coupling constant ν_Q differs between 60 MHz and 100 MHz and the asymmetry parameter of the field gradient varies from smaller than 0.05 to 0.19.

The more recent work [2], [11] seems to indicate that there is only one defect complex which is structurally identical in all II-VI compounds, but these results are found in samples with lower dopant concentrations than the samples in earlier publications [9], [10].

1.3. OUTLINE OF THE PROJECT

Indium has a very strong quadrupole interaction, partly because of its large quadrupole moment (Q~1.15 barns) partly due to the large number of surrounding electrons. These two features may make it difficult to observe the quadrupolar shifted lines in NMR spectra. It is expected that gallium, which is chemically identical and only a smaller nucleus, exhibits similar behavior as a dopant and its smaller quadrupole moment (Q~0.14 barns) and lower number of electrons should make it easier to find the resonances using NMR. PAC measurements in these materials

are favorably done on indium because it has a radioactive isotope with a suitable lifetime and decay process.

The goal of this project is to measure and specify the local environment of group III dopants in CdTe. The local structure of the site of the dopants e.g. its electronic structure and its symmetry should be accessible by measurements of the quadrupolar interaction, which has an orientational dependence in single crystals and a characteristic pattern in powders. This work is done on CdTe samples doped with indium or gallium. The samples are either single crystals or powders.

NMR measurements on the host nuclei and the impurities should yield the dominant relaxation processes for the individual species and thus provide information about the interaction between the spins and the lattice. The magnetic shift of the resonance line and the relaxation time may allow the specification of the number of non-localized electrons for different dopants, different concentrations and at different temperatures.

The use of NMR as a technique to gather information on a microscopic scale in CdTe will complement the PAC measurements. NMR is most sensitive to sites with no or with a small quadrupole interaction while PAC emphasizes sites with a large electric field gradient.

2. BASIC CONCEPTS OF NUCLEAR MAGNETIC RESONANCE

2.1. ZEEMAN ENERGY

Almost all elements have at least one isotope which possesses a nuclear spin $\overrightarrow{I}$. This spin $\overrightarrow{I}$ can be measured with respect to a certain axis, its projection is quantized and takes on integer and half integer values only. The nuclear spin $\overrightarrow{I}$ is described by a quantum number I, which is the same for all nuclei of a certain isotope. Associated with the quantum number I is a magnetic quantum number m_I, which can take on $m_I = -I, -I+1, ..., I-1, I$ as possible values. Those nuclei have a magnetic dipole moment $\overrightarrow{m}$ given by the relation

$$\overrightarrow{m} = g_N \mu_N \overrightarrow{I} = \gamma \hbar \overrightarrow{I}, \tag{2.1}$$

where $\hbar \overrightarrow{I}$ is the angular momentum. The projection of these moments along a certain axis z, can take on the values

$$\left(\overrightarrow{m}\right)_z = \hbar \gamma m_I \ , \tag{2.2}$$

where γ is the gyromagnetic ratio, i.e. the ratio between the magnetic dipole moment and the angular momentum $\hbar \overrightarrow{I}$ of the nuclear spin $\overrightarrow{I}$. The gyromagnetic ratio γ is a product of two numbers, the nuclear magneton μ_N divided by $\hbar$ and the gyromagnetic factor g_N. The nuclear magneton μ_N is the ratio of the magnetic moment $\overrightarrow{m}$ and the nuclear spin $\overrightarrow{I}$, if one models the spin as a charge circling on a current loop, therefore having an angular momentum $\hbar \overrightarrow{I}$ and producing the

magnetic moment $\overrightarrow{m}$. The gyromagnetic factor g_N corrects for relativistic effects, not being accounted for in this model.

In a magnetic field $\overrightarrow{B}$ a nucleus with a magnetic dipole moment has the Zeeman energy

$$E = -\overrightarrow{m} \cdot \overrightarrow{B} = -\hbar\gamma B m_I \,. \tag{2.3}$$

There are $2I + 1$ different energy levels, they are equally spaced and transitions between them have to obey the selection rules. Therefore in one photon processes only transitions with $\Delta m_I = \pm 1$ are allowed. The frequencies of the photons absorbed or emitted in these transitions are typically in the range between $10^7 - 10^9$ Hz in magnetic fields of 1 to 10 Tesla. This allows one to induce transitions between these states using radiofrequency photons.

The Zeeman energies are characteristic for the nuclei under investigation and are linear in the applied magnetic field. However in real materials these energy levels are often perturbed by hyperfine interactions produced by the environment of the nucleus. If one wants to calculate the effect of the hyperfine interactions on the energy levels, one has to choose the appropriate method, i.e. if the perturbations are small compared to the splitting of the Zeeman levels one can use perturbation theory. Otherwise a simultaneous diagonalization of the whole Hamiltonian is required.

2.2. THE EFFECT OF AN APPLIED FIELD

This is a short explanation of the effect of a resonant applied radiofrequency field $\overrightarrow{B_1}$ on a spin system which is in thermal equilibrium with the static magnetic field $\overrightarrow{B_0} = (0, 0, B_0)$. One may refer to [12, ch.2].

The magnetic moment $\overrightarrow{m}$ of a spin, which is related to the angular momentum of the spin (2.1), experiences a torque $\overrightarrow{\tau} = \overrightarrow{m} \times \overrightarrow{B_0}$ in a magnetic field

$\overrightarrow{B_0}$. Classically this torque equals the rate of change of angular momentum $\frac{d(\hbar \overrightarrow{I})}{dt}$. Using 2.1 we can replace the angular momentum $\hbar \overrightarrow{I}$ and get a differential equation for the motion of the magnetic moment

$$\frac{d\overrightarrow{m}}{dt} = \overrightarrow{m} \times (\gamma \overrightarrow{B_o}). \tag{2.4}$$

This holds whether the magnetic field is time dependent or not. The motion of $\overrightarrow{m}$ is described by a vector precessing around the magnetic field with its tail on the axis of the field and its tip moving along a circle with the center on the field axis. Thus its motion is defining a cone with its axis parallel to the field.

In the case of many spins, i.e. of many magnetic moments in the same magnetic field, all of them precess in the field around the same axis, but à priori each of them has its own phase with respect to the x-axis. Therefore the sum over the individual components m_x^i, m_y^i, m_z^i, where i goes over all nuclei, yields the macroscopic magnetization $\overrightarrow{M}$, of which only the z-component is different from zero. This is true as long as the spin system hasn't been prepared in a special way. Thus a sample of nuclei with nonzero spins in a magnetic field has a macroscopic magnetization $\overrightarrow{M}$ pointing along the axis of the field.

The precession frequency of the individual magnetic moment $\overrightarrow{m}$ in a magnetic field is given by

$$\overrightarrow{\omega_L} = -\gamma \overrightarrow{B}, \tag{2.5}$$

the so called Larmor frequency. One can imagine sitting on a reference frame with its z'-axis coinciding with the laboratory frame (LAB) z-axis and its x' and y'-axes rotating in the x-y-plane of the LAB with an angular velocity $\overrightarrow{\omega}$, which is exactly the Larmor frequency. The spins rotating around the magnetic field $\overrightarrow{B_0}$ would then appear to be static. If one applies an additional magnetic field $\overrightarrow{B_1}$ rotating in the

x-y-plane with the Larmor frequency all the spins experience is a static field $\overrightarrow{B_1}$ in the x'-y'-plane, since they are already reacting on the static field $\overrightarrow{B_0}$ by their precessional movement. The torque generated by $\overrightarrow{B_1}$ now forces them to precess around the field $\overrightarrow{B_1}$ according to 2.4 with a frequency $\overrightarrow{\omega}$, again given by 2.5.

Usually, the radiofrequency field $\overrightarrow{B_1}$ is linearly polarized and applied along an axis in the x-y-plane of the laboratory frame. In fact the rotational symmetry around the z-axis is broken only by the application of $\overrightarrow{B_1}$ and this distinguishes the x-axis from all other directions in the x-y-plane.

A linearly polarized oscillation of frequency ω can be represented as a superposition of two circularly polarized waves; one of them rotating clockwise and the other one rotating counterclockwise with the frequency ω. The influence of the component rotating in the opposite sense as the spins can be neglected, while the component rotating in the same sense can cause the macroscopic magnetization $\overrightarrow{M}$ to rotate around the momentary direction of this component. This causes the magnetization to turn into the x-y-plane of the rotating frame.

The magnetization will turn by an angle Θ, given by

$$\Theta = \omega \cdot t = \gamma \cdot B_1 \cdot t, \tag{2.6}$$

and by applying the field $\overrightarrow{B_1}$ for a certain time t one can control Θ. It allows one to invert the macroscopic magnetization $\overrightarrow{M}$ ($\Theta = \pi$) or to bring it into the x-y-plane ($\Theta = \frac{\pi}{2}$) of the two reference frames. $\overrightarrow{M}$ is now precessing in the x-y-plane of the LAB frame. This time dependent magnetic moment can be detected by a coil located in the plane. The amplitude of the induced current is proportional to the amplitude of the magnetization $\overrightarrow{M}$.

2.3. THERMAL EQUILIBRIUM AND RELAXATION

2.3.1. Thermal Equilibrium

To nuclei with a spin $\overrightarrow{I}$ in a magnetic field there are $2I+1$ possible energy levels available (2.3). The distribution of the spins among these levels is not a trivial matter since the spins can obey several statistics: Fermi-Dirac statistics, if they are identical fermions, Einstein-Bose statistics in case of bosons and finally Boltzmann statistics in the high temperature limit. The high temperature limit is valid if the thermal energy kT is larger than the Zeeman energy of the spins. In the case of nuclear moments in magnetic fields of 10 Tesla this is true down to about 10 mK [12, p.63].

It is easier to deal with the total energy of the system, which is just the sum over all individual spin energies. An ensemble of spin systems obeys the Boltzmann statistics. If the system has got a set of possible energies E_i, it will occupy these levels with the probabilities $p(E_i)$

$$p(E_i) = \frac{e^{-E_i/kT}}{Z}, \tag{2.7}$$

where Z is the partition function $\sum_i \exp(-E_i/kT)$ and is a constant at a fixed temperature T. The probabilities are normalized

$$\sum_{E_i} p(E_i) = 1.$$

In thermal equilibrium the ratio between populations of different states is just the ratio of two exponentials and all systems which obey this distribution can be described by the spin temperature T in 2.7. In cases in which more of the higher than of the lower energy levels are occupied this doesn't hold anymore. For example, if we prepare the system in a state in which its magnetization $\overrightarrow{M}$ lies in the x-y-plane the

number of states with spin along the field must equal the number of states with spin opposing the field. The probabilities of 2.7 can not be used to describe this situation unless the spin temperature T is infinite. In the case of an inverted magnetization $\overrightarrow{M}$, the situation can be described by a negative temperature.

If we assume a coupling among the spins they will relax towards a Boltzmann equilibrium distribution. In case of a strong coupling they will do so relatively fast compared to the time needed for the energy transfer from the spin system to the lattice to achieve thermal equilibrium throughout the sample. Thus the temperature of this internally relaxed spin system doesn't have to match the lattice temperature.

2.3.2. Spin-Lattice Relaxation Time T_1

The static magnetic field $\overrightarrow{B_0}$ breaks the symmetry, i.e. the isotropy of space. Energetically it makes a difference for the spins whether they point along the z-axis or opposite to it. There is no such difference in their orientation within the x-y-plane. Intuitively it seems obvious that there must be two time constants describing relaxation in such a system. One constant describes a relaxation in which energy transfer is involved, the so called spin-lattice relaxation. The other relaxation leaves the total energy of the spin system unaltered and is called spin-spin relaxation.

Spin-lattice relaxation is mediated by processes in which energy is exchanged between the spin system and the lattice, i.e. whenever a spin changes its orientation in the field and looses the energy ϵ the lattice has to make a transition from a low energy state to one higher by the amount ϵ.

An example for such a process is the relaxation by conduction electrons. A transition of a spin yields the energy $E = -\gamma\hbar B\Delta m$ (2.3) typically smaller than 5 μeV. This energy can be absorbed by electrons on the Fermi surface only, since all

other electrons are blocked by the Pauli exclusion principle. Furthermore the Fermi surface has to lie inside an electron band of the material, since 5 μeV are not enough to cause interband transitions.

The spin-lattice relaxation is described by a linear differential equation in time, which has an exponential as a solution and the time constant is the spin-lattice relaxation time T_1. After about five times T_1 the spin system is essentially in thermal equilibrium with the lattice and the equilibrium magnetization $\overrightarrow{M}$ is reestablished.

2.3.3. Spin-Spin Relaxation Time T_2

After one has applied a resonant magnetic field $\overrightarrow{B_1}$ the phase of the individual spins with respect to each other is no longer unspecified. By turning the magnetization $\overrightarrow{M}$ by an angle Θ one picks a special phase configuration of the spin system. The phases which were randomly distributed as long as $\overrightarrow{M}$ pointed along the z-axis remain random but now only with respect to the new direction of $\overrightarrow{M}$. The spins show a non-random distribution with respect to the LAB frame, i.e. they all point into the half space of the axis onto which $\overrightarrow{M}$ was rotated. This is unusual, since it is a highly ordered state, which isn't forced to exhibit this order by any kind of potential. In order to increase the entropy of the spin system it is necessary for the spins to dephase, i.e. to loose their phase correlation. This process can be described by an exponential with a characteristic relaxation time T_2. It is important to realize that the total energy of the spin system is conserved in this relaxation.

One dephasing mechanism is the dipole-dipole interaction in which one magnetic dipole (spin) causes a deviation from the externally applied field $\overrightarrow{B_0}$ at the site of another nuclei. This causes the spin to precess a little faster or slower than its neighbors. Since there will be a distribution of local fields, all the spins will precess

at slightly different angular velocities. The spins dephase but a definite relation between their phases remains unless the dipoles which cause the dephasing fluctuate randomly. The energy required for these fluctuations (≤ 5 μeV) can be provided thermally down to very low temperatures.

2.4. HYPERFINE INTERACTIONS

According to Mehring [13] there are seven ways in which a nuclear spin system of a solid can interact with its surrounding. The spins can directly interact with an externally applied magnetic field, or they interact internally, i.e. with each other or properties of the sample like electrons or phonons. Therefore the Hamiltonian describing the nuclear spin interactions splits into two parts

$$H = H_{ext} + H_{int} \tag{2.8}$$

where $H_{ext} = H_0 + H_1$ describes the Zeeman interaction and is much larger than internal interactions. The six internal interactions are in general given by

$$H_{int} = H_{II} + H_{SS} + H_{IS} + H_Q + H_S + H_L. \tag{2.9}$$

where I, S are spins of different kind.

H_{II} and H_{SS} represent direct dipolar as well as indirect (via electrons) interactions among I spins and S spins respectively. H_{IS} represents the same interactions among different kind of spins. H_Q is the quadrupole Hamiltonian of the nucleus, i.e. the interaction of its quadrupole moment with an external charge distribution. H_S contains the shielding of the spins I, S from the external fields by the electronic configuration of the sample (chemical shift, Knight shift). H_L describes the spin-lattice interaction, which is either direct interaction of the spins I, S with phonons or indirect coupling via electrons to the lattice.

The Hamiltonian H is in general time-dependent since usually at least the applied radiofrequency field $\overrightarrow{B_1}$ is varied in an experiment. The time independent parts of the internal Hamiltonian H_{int} produce a shift of the resonance line if they alter the Zeeman energy levels. The time dependent parts of the internal Hamiltonian H_{int} cause relaxation processes, i.e. they cause transitions between different states of the system.

Nuclear magnetic resonance allows us to gather information about the local environment of the nuclei under consideration by measuring the effect of the internal Hamiltonian H_{int} on the Zeeman levels of the system. At least the average environment of the isotope under consideration is accessible and its static and dynamic characteristics can be measured.

2.5. HAMILTONIAN OF QUADRUPOLAR INTERACTIONS

In this section the quadrupolar Hamiltonian H_Q will be discussed briefly. One may also refer to [14].

2.5.1. The Hamiltonian H_Q

The electrical charge of the nucleus is distributed over a certain volume, this yields a charge distribution $\rho(\overrightarrow{x})$. This charge distribution sits in an electrostatic potential, which is due to all charges other than those of the nucleus itself. The electrostatic energy of a charge distribution in an electrostatic potential is

$$H_{el} = \int \rho(\overrightarrow{x}) V(\overrightarrow{x}) d^3x.$$

The electrostatic potential $V(\overrightarrow{x})$ is not constant within the volume of the nucleus and so one expands the energy in multipoles [15, p.138]. This procedure yields for the quadrupolar energy

$$H_Q = \frac{1}{6}\sum_{j,k} Q'_{jk} V_{jk} \ . \tag{2.10}$$

Thus the nuclear electric quadrupole moment interacts with the gradient of the electric field, i.e. the V_{jk} are the elements of the electric field gradient tensor $\tilde{V}$. Q'_{jk} are the elements of the electric quadrupole moment tensor $\tilde{Q}$ expressed in Cartesian coordinates. It is symmetric and thus has six independent components. It is defined as

$$Q'_{jk} \equiv \int \rho\left(\overrightarrow{x}\right) x_j x_k d^3x,$$

but it is possible to define a more convenient traceless quadrupole moment tensor, without changing its orientational properties

$$Q_{jk} = 3Q'_{jk} - \delta_{jk}\sum_e Q'_{ee} \ .$$

According to the Wigner-Eckhart Theorem all corresponding matrix elements of all traceless, second rank, symmetric tensors are proportional, i.e.

$$\langle I, m' \mid Q_{jk} \mid I, m\rangle = C\langle I, m' \mid \frac{3}{2}(I_j I_k + I_k I_j) - \delta_{jk}\overrightarrow{I}^2 \mid I, m\rangle \ , \tag{2.11}$$

so that one can relate all the matrix elements of the operator of the quadrupolar interaction 2.10 to well defined matrix elements of the angular momentum operator $\overrightarrow{I}$. Using a special case of 2.11 and defining a quadrupole moment Q

$$eQ \equiv \langle II \mid Q_{zz} \mid II\rangle = C\langle II \mid 3I_z^2 - \overrightarrow{I}^2 \mid II\rangle,$$

one finds for the proportionality constant

$$C = \frac{eQ}{I(2I-1)}.$$

The components of the electric field gradient tensor $\tilde{V}$ are the second derivatives of the potential in Cartesian coordinates at the site of the nucleus

$$V_{jk} = \frac{\partial^2 \tilde{V}}{\partial x_j \partial x_k}.$$

This tensor is clearly symmetric, i.e. $V_{jk} = V_{kj}$. The electric field gradient tensor $\tilde{V}$ must be traceless, since there are no external charges at the site of the nucleus and thus the Laplace equation holds

$$\nabla^2 \tilde{V} = V_{xx} + V_{yy} + V_{zz} = 0. \tag{2.12}$$

In the principal axis system (PAS) of the electric field gradient tensor $\tilde{V}$, there are only two independent components left, since all off-diagonal elements of a symmetric tensor vanish in its PAS. One usually defines the order of the axes in the PAS by $| V_{z'z'} | \geq | V_{y'y'} | \geq | V_{x'x'} |$, and further

$$\begin{aligned} eq &\equiv V_{z'z'} = \tfrac{\partial^2 V}{\partial z'^2} \,|_{nuclei} \\ \eta &\equiv \tfrac{V_{x'x'} - V_{y'y'}}{V_{z'z'}}, \end{aligned} \tag{2.13}$$

so that $0 \leq \eta \leq 1$. The primed indices represent the PAS. The most general electric field gradient is thus specified by the orientation of its PAS with respect to the LAB, i.e. three Eulerian angles, and the two parameters eq and the asymmetry parameter η. These are five parameters, which is exactly the number of independent components of a general symmetric, traceless tensor of rank two.

Finally by plugging these definitions into 2.10 one gets to the following form of the quadrupolar Hamiltonian H_Q in the PAS $\left(x', y', z'\right)$of the electric field gradient tensor (Abragam [16, p.166], Slichter [12, p.496])

$$\begin{aligned} H_Q &\overset{Abragam}{=} \tfrac{e^2 qQ}{4I(2I-1)} \left\{ 3I_{z'}^2 - I(I+1) + \tfrac{1}{2}\eta(I_{+'}^2 + I_{-'}^2) \right\} \\ &\overset{Slichter}{=} \tfrac{eQ}{4I(2I-1)} \left[V_{z'z'}(3I_{z'}^2 - I^2) + (V_{x'x'} - V_{y'y'})(I_{x'}^2 - I_{y'}^2) \right], \end{aligned} \tag{2.14}$$

where $I_{\pm'} = I_{x'} \pm i I_{y'}$ are the raising and lowering operators of the angular momentum with respect to the PAS.

2.6. ORIENTATIONAL DEPENDENCE OF QUADRUPOLE SHIFTS

2.6.1. The General Case

The quadrupolar Hamiltonian H_Q as given in 2.14 depends on the orientation of the PAS of the field gradient tensor with respect to the external field $\overrightarrow{B_0}$. The primed angular operators apply in the PAS, but in case of a dominant magnetic field B_0 the angular momentum remains quantized along the z-axis of the laboratory frame, i.e. as long as $\langle H_Q \rangle \ll \langle H_0 \rangle$ a solution for the energy levels of the system can be calculated by perturbation theory. This requires a rotational transformation of the Hamiltonian H_Q into the LAB frame and is done in several standard textbooks [16], [12], [17] for the case of a symmetrical field gradient, i.e. $\eta = 0$.

The case of a non-axial field gradient is a little more complicated but the solution is given in [18]. The Larmor frequency $\nu_L = \omega_L/2\pi$ is perturbed in first and second order by the frequency shifts $\nu^{(1)}, \nu^{(2)}$ respectively, so that the observed frequency is given by $\nu_{obs} = \nu_L + \nu^{(1)} + \nu^{(2)}$. The perturbation terms are given by

$$\nu^{(1)}_{m\to m-1} = \nu_Q \frac{1}{2}(m - \frac{1}{2})(3\cos^2\beta - 1 - \eta\cos 2\alpha \sin^2\beta), \tag{2.15}$$

and

$$\begin{aligned}\nu^{(2)}_{m\to m-1} = \tfrac{\nu_Q^2}{12\nu_L} \quad & \{\tfrac{3}{2}\sin^2\beta\,[(A+B)\cos^2\beta - B] \\ & +\eta\cos 2\alpha \sin^2\beta\,[(A+B)\cos^2\beta + B] \\ & +\tfrac{\eta^2}{6}\,[A - (A+4B)\cos^2\beta - (A+B)\cos^2 2\alpha(\cos^2\beta - 1)^2]\}\end{aligned} \tag{2.16}$$

The coefficients are

$$\begin{aligned} A &\equiv 24m(m-1) - 4I(I+1) + 9 \\ B &\equiv \tfrac{1}{4}\,[6m(m-1) - 2I(I+1) + 3] \\ \nu_Q &\equiv \tfrac{3e^2qQ}{2I(2I-1)\hbar}. \end{aligned} \tag{2.17}$$

The angles α, β are the Eulerian angles used to bring the z'-axis of the PAS in coincidence with the z-axis of the LAB frame. The angle α is the angle by which one rotates the PAS around the z'-axis to bring the x'-axis onto the line of intersection of the x'-y'-plane of the PAS with the x-y-plane of the LAB frame. This yields the new axis x'_1. A following rotation by β around x'_1 turns z' onto the z-axis, the axis of the static magnetic field $\overrightarrow{B_0}$. A third rotation around the z-axis is not necessary, since the angular momentum is quantized with respect to this axis and rotation around the quantization axis doesn't change the energy levels.

2.6.2. An Example

This is a rough estimate for the resonance frequencies expected for indium nuclei in CdTe complexed with a Cd vacancy using data reported from PAC measurements. Since the quadrupolar interaction energies and the coupling constant are very high ($\frac{e^2qQ}{h} = 60$ MHz) a simultaneous diagonalization of the Zeeman Hamiltonian and the quadrupolar Hamiltonian is required for an exact solution but this would mean to diagonalize a $(2I+1) \times (2I+1)$ matrix. In case of ^{115}In this would be a 10×10 matrix. However the above perturbation approach will give us a handle on what to expect for the quadrupolar shifts and in which range one has to look for NMR resonances. The inclusion of higher terms in the perturbation expansion would converge to the exact result.

^{115}In has a nuclear spin of $I = \frac{9}{2}$ and a natural abundance of 95%, so that only this isotope is of interest here. The coefficients in 2.17 for the central transition $m = \frac{1}{2} \rightarrow m = -\frac{1}{2}$ are $A = -96$ and $B = -12$. The coupling constant experienced by the radioactive ^{111}Cd PAC probe nuclei is $e^2qQ/h = 60$ MHz as reported in [2]. The asymmetry parameter η is reported to be $\eta = 0.09$ and here assumed to be

zero. An inclusion of η in this estimate is not possible since the orientation of $V_{x'x'}$ with respect to the zinc blende structure of CdTe is not reported. In order to find η and the missing angle α one would fit 2.16 to the results of a measurement.

The component $V_{z'z'}$ of the field gradient lies along the $\langle 111 \rangle$ direction of the cubic cell in CdTe. One has to take the different quadrupole moments of the different probe nuclei into account and a calculation of the quadrupole frequency shift $\nu_Q = \frac{3}{2I(2I-1)} \frac{e^2qQ}{h}$ yields

$$\nu_Q^{In} = \frac{3}{2I_{In}(2I_{In}-1)} \cdot \frac{Q_{In}}{Q_{Cd}} \cdot 60 \text{ MHz} \approx 3.6 \text{ MHz}.$$

This should hold as long as the Sternheimer antishielding factor γ_∞ doesn't change a lot by the use of different probe nuclei, which is not expected since indium and cadmium are of about the same size and almost identical electronic configuration. The use of γ_∞ is appropriate if the charge distribution which causes the electric field gradient doesn't overlap with the electron shells of the probe nuclei. This holds according to the PAC publications. The values for the Sternheimer antishielding factor are $\gamma_\infty = -28$ for ^{115}In and $\gamma_\infty = -31.9$ in case of ^{111}Cd [19, p. 54], but their effect is not taken into account in this example. If anything their inclusion would result in a smaller shift of the resonance frequency.

The frequency shift with respect to the Larmor frequency for a central transition is then found to be (from 2.15, 2.16 and using $\nu_L(^{115}\text{In } at \text{ 8 T}) = 74.64$ MHz)

$$\Delta\nu \approx 0.022 \sin^2\beta \left(12 - 108\cos^2\beta\right) \text{ MHz}. \tag{2.18}$$

The angular dependence of the shift can be exploited if one measures the resonance frequency at different orientations of the sample with respect to the LAB frame. In a typical experiment one is confined to rotations in the LAB frame, for example

around the axis of the coil i.e. the x-axis. A vector transforms under a rotation around the x-axis by an angle δ according to

$$\overrightarrow{k}' = \tilde{R}\,\overrightarrow{k},$$

where the rotation matrix $\tilde{R}$ is given by

$$\tilde{R} = \begin{pmatrix} 1 & 0 & 0 \\ 0 & \cos\delta & \sin\delta \\ 0 & -\sin\delta & \cos\delta \end{pmatrix},$$

and δ is in the mathematical positive sense. If we start from a configuration in which $V_{z'z'}$ points along the $\langle 111 \rangle$ direction in the LAB frame the angle $\beta = \arccos\left\{k_z/|\overrightarrow{k}|\right\}$ between $V_{z'z'}$ and the z-axis changes as a function of rotation angle δ according to

$$\begin{aligned} \cos^2\beta &= \tfrac{1}{3}\left[1 - 2\cos\delta\sin\delta\right] \\ \sin^2\beta &= \tfrac{1}{3}\left[2 + 2\cos\delta\sin\delta\right] \end{aligned}$$

Thus 2.18 is found to be

$$\Delta\nu_Q = \frac{0.022}{3}\left[2 + 2\cos\delta\sin\delta\right]\left\{12 - \frac{108}{3}\left[1 - 2\cos\delta\sin\delta\right]\right\}\ \text{MHz}\ , \qquad (2.19)$$

and plotted in figure 2.1.

This estimate justifies the use of NMR in the search for resonances of ^{115}In on substitutional sites in CdTe single crystals, since the quadrupolar shift of the central transition is expected to be smaller than 0.5 MHz. This relatively small shift allows one to scan the frequency around the ^{115}In resonance frequency. One has to keep in mind however that 2.19 is only an estimate and the real shift could be by a factor of two or three bigger.

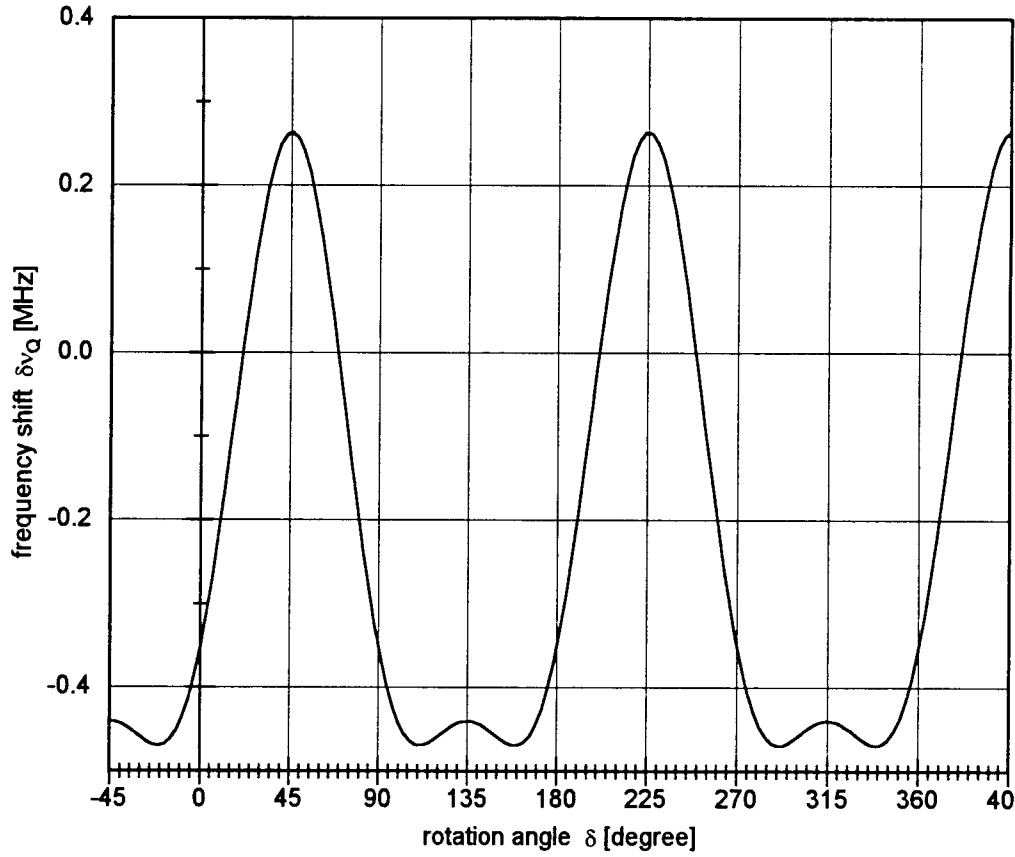

Frequency shift of the central transition of ^{115}In in an axial field gradient (ν_Q=3.6MHz, ν_L=74.64MHz) along the <111> direction of a zinc blende structure as a function of rotation around the x-axis.

FIG. 2.1. Rotational Pattern for an Axial Field Gradient

3. DETAILS OF THE EXPERIMENT

3.1. THE SAMPLES

All of the single crystal samples were provided by Ursula Debska Bindley. She is working for Prof. J. K. Furdyna at the University of Notre Dame, Physics Department, Notre Dame, Indiana 46556, USA.

They were grown using the Bridgman technique in which the ingredients are encapsulated in a quartz ampoule and heated above their melting point. The ampoule is then lowered through a temperature gradient to a region with a temperature below the melting point of CdTe. Single crystals of several centimeters length with the diameter of the ampoule can be achieved. The growth axis of zinc blende structure usually is the $\langle 111 \rangle$ direction. We were not provided with information about the orientation of the samples.

3.1.1. Sample 1

Sample 1 ($Cd_{.99}In_{.01}Te$, i.e. CdTe: In $1.5 \times 10^{20} cm^{-3}$) is an indium-doped single crystal of cadmium telluride. It is doped to one atomic percent and is about 1.5 cm long and about 1 cm in diameter. It was subsequently oriented by X-ray diffraction and cut into a cube of 0.5 cm edge length and $\langle 100 \rangle$ faces at a commercial laboratory*. The concentration of free carriers was not determined for this sample.

---

*Since CdTe crystals are very brittle, this is not a trivial task and was done at: Virgo Optics, 6736 Commerce Avenue, Port Ritchey, Florida 34668

3.1.2. Sample 2

Sample 2 (CdTe: In $1 \times 10^{19}\text{cm}^{-3}$) is an indium-doped single crystal of cadmium telluride. It is about 1.4 cm long and 0.8 cm in diameter. It was not oriented or cut. The concentration of free carriers was measured† and found to be $n = 3.5 \times 10^{17}\text{cm}^{-3}$ at $T = 300$ K and $T = 80$ K. These values are a little lower than expected from Ref. [6, fig. 8] but considering the strong dependence of the carrier concentration on the annealing procedures [7] this deviation is not surprising.

3.1.3. Sample 3

Sample 3 (CdTe: Ga $1 \times 10^{19}\text{cm}^{-3}$) is a gallium-doped single crystal of cadmium telluride. It is about 1.5 cm long and 0.8 cm in diameter. It was not oriented or cut. The concentration of free carriers is $n = 2.5 \times 10^{15}\text{cm}^{-3}$ at $T = 330$ K and $n = 9 \times 10^{14}\text{cm}^{-3}$ at $T = 83$ K. The lower carrier concentration can be interpreted as due to a lower energy level of the gallium dopant in the gap. That is, gallium is not as shallow a donor as indium. Precise data on the energy levels in the gap are not available.

3.1.4. Sample 4

Sample 4 is commercially available CdTe-powder from Johnson Matthey Electronics of 99.999% purity.

---

†The Hall measurements on sample 2 and sample 3 were done by N.G. Semaltionos in Prof. Furdyna's group.

3.1.5. Sample 5

Sample 5 is a randomly shaped single crystal of undoped cadmium telluride cleaved out of a larger rod like single crystal. It was grown with the same technique as samples 1, 2, 3 and supplied by the same source. It has a high resistivity and a mass of 0.82 g.

3.1.6. Powder Samples

A powder sample of pieces of sample 2 and a self-produced powder sample of gallium diffusion-doped CdTe were used to find resonances of the dopants.

3.1.7. Reference Samples

A liquid solution of gallium chloride in distilled water at various concentrations was used as an NMR shift reference for gallium in sample 3. The reference didn't shift with different concentrations. The exact concentration of the solution is not known since gallium chloride is highly hygroscopic.

Cadmium salts dissolved in water display a strong dependence of the cadmium resonance frequency on the concentrations. I used a 0.1 molar solution of $CdSO_4$ in distilled water as a reference for cadmium. $CdSO_4$ has the lowest concentration dependence and its resonance is only shifted by 0.1 ppm with respect to an infinitely dilute sample [20, table 1].

3.2. THE APPARATUS

3.2.1. The Spectrometer

The CMX360-1436 is a commercially available spectrometer built by Chemagnetics, Inc. It has two independent radio-frequency channels, which allows double resonance. One of the channels is set up for proton NMR, both of the channels use frequencies generated by PTS 500 frequency synthesizers, which range from $1 - 500$ MHz. The generated pulses are amplified by two linear rf pulse amplifiers of the 3000 series from American Microwave Technology, Inc.

Using quadrature detection two NMR signals which are ninety degrees out of phase are achieved.

The minimal dwell time between the digitization of two points of the signal is 500 ns, so that the maximum detectable spectral range is $\nu_{sf} \pm 1$ MHz where ν_{sf} is the applied spectrometer frequency.

The Fourier transformations were done on a IBM compatible PC using a Fast Fourier transformation algorithm.

3.2.2. The Magnet

The magnet is a superconducting magnet built by American Magnetics, Inc. It is cooled by liquid helium and has a 3 inches room temperature clear bore. It has a central field of 8 Tesla with maximum homogeneity of 1 ppm over a 1 cm diameter spherical volume. This corresponds to a line width of 100 Hz at a resonance frequency of 80 MHz.

3.2.3. The Temperature Control

For these experiments the temperature can be varied continuously from −65° C to 200° C using a gas flow system supplied by the spectrometer manufacturer.

3.2.4. The Coil, the Quality Factor and the $\frac{\pi}{2}$-Pulse

The coil used in most of the experiments is 1 cm long and has an inner diameter of 8 mm. It has six turns. A $\frac{\pi}{2}$-pulse on ^{69}Ga can be achieved within 7.0 μs and for ^{115}In it takes 7.5 μs to rotate the magnetization by $\frac{\pi}{2}$ into the transverse plane. Both pulse widths were measured in non conducting samples. Using Eq. 2.6 one can solve for the transverse field $\overrightarrow{B_1}$ and finds an amplitude of $B_1 = 3.5 \times 10^{-3}$ Tesla for the field.

The probe is made of two variable capacitors and a coil with an inductance. The coil is parallel to one of the capacitors, the so called tuning capacitor ($C = 0.5 - 10$ pF). This resembles an LC-circuit which can store power in the alternating magnetic and electric fields radiated by the coil and in the electric field of the capacitor. The better this resonant circuit is tuned the more energy it can store in the fields and the more energy can be absorbed by the NMR sample. Proper tuning is achieved when a minimum of energy is reflected back into the amplifiers and maximum energy is radiated onto the sample. One way to measure optimal tuning is by looking at the reflected voltage which should be at a minimum. One side of the parallel circuit is grounded, the other side is in series with the so called matching capacitor ($C = 0.5 - 5pF$) which is needed to adjust the impedance of the probe to the 50 Ω impedance of the BNC cables.

The quality factor Q of the coil is defined as the maximum energy stored in a coil times the frequency divided by the power which is dissipated in the resistance of

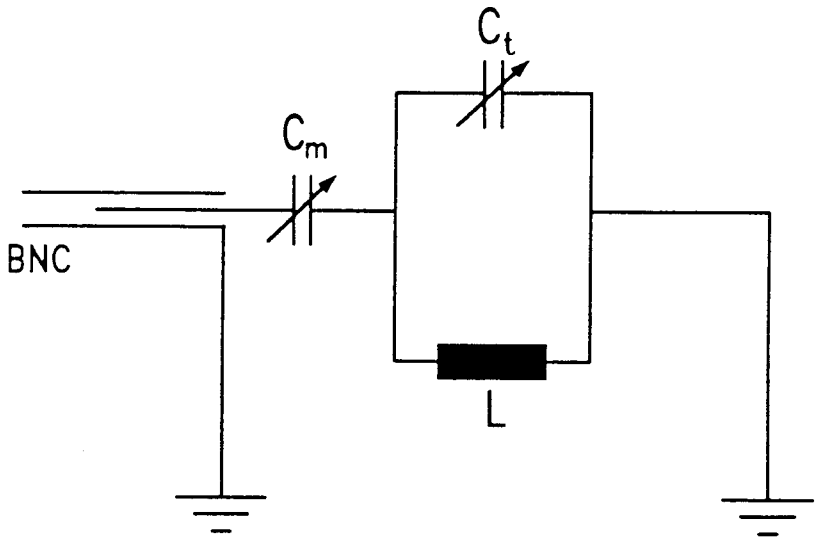

FIG. 3.1. Resonance Circuit of the Probe

the coil. In the case of a high Q factor a lot of energy can be provided to the sample and also small fields can be detected very effectively, since the resistance is small. One drawback is the long ring down time of the coil, caused by a small resistance and small losses. One way to measure Q is to tune the probe at a certain frequency and then change the frequency without retuning. One then records the reflected voltage and the supplied voltage. If one plots $(V_{reflected}/V_{input})^2$ versus frequency ν, Q can be gained by dividing the width of the resonance curve at half maximum by the frequency at which the probe is tuned.

The coil used has a quality factor Q of about 120-130 between $74 - 82$ MHz. The resonance curve for the probe tuned at $\nu = 81.776$ MHz is plotted in figure 3.2.

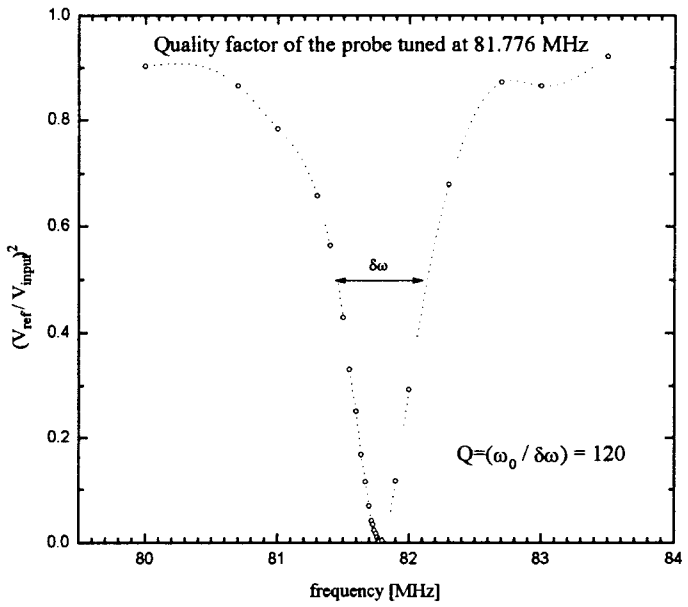

FIG. 3.2. Resonance Curve of the Tuned Probe

3.3. THE MEASUREMENTS

3.3.1. The Skin Effect

NMR measurements on conducting materials face the problem of the skin effect. Conductors expel electromagnetic waves, i.e. the amplitude of an alternating magnetic field dies off exponentially with the distance from the surface of the material. The depth at which the wave is attenuated to $\frac{1}{e}$ of its amplitude at the surface of the sample is the skin depth. It is given by

$$\delta = \sqrt{\frac{2}{\mu\omega\sigma}}, \tag{3.1}$$

in SI units [15, p. 298], where σ is the conductivity, ω is the frequency and μ is the permeability. The higher the frequency ω, the smaller the skin depth δ.

Due to the skin effect the applied magnetic field B_1 cannot be homogeneous throughout the volume of the sample. Thus the time t needed to turn the magneti-

zation by an angle Θ is not equal for all regions of the sample. A true π-pulse can therefore not be achieved and use of those echo sequences which involve a π-pulse is not possible.

An additional problem may be caused by eddy currents induced by the rf field. After the rf pulse has been applied these currents die off slowly and may be picked up in the beginning of an NMR time signal. This ringing of the sample has to be cut off and one looses the possibility to pick up signal relatively soon after the application of the pulse. Signals from nuclei with a short spin-spin relaxation T_2 or with a short dephasing time constant T_2^* may be hidden by an overlay of the sample ringing.

These problems are usually avoided by the use of powdered samples, where the grain size is small compared to the skin depth. In this work this is not possible since the use of powders would result in powder patterns in which the intensity of the signals is spread over a wide frequency range. Since this work is done on impurities at low concentrations compared to the host nuclei the intrinsic intensity is already small. Remember also that figure 2.1 is only an estimate and might be off by a factor of two or three i.e., if the shift would be larger, a powder pattern could be as wide as 3 MHz. It would become very difficult to measure it for two reasons.

First of all the width of the powder pattern would be large compared to the pulse spectrum, so that the total line might not even get excited. This could be avoided by very short pulses, but then intensity would be very low because the component of the magnetization in the transverse plane would be small. Therefore an unreasonably long signal averaging would be required.

Second and more serious, it would also be impossible to pick up very wide lines due to the resonance curve of the probe (figure 3.2), i.e. if the line is wider than the resonance curve at half maximum.

In order to measure a spectrum which is wide compared to the pulse spectrum or the resonance curve of the probe one would need to scan the spectrum by varying the spectrometer frequency. The measurement of a number of points would also require a prohibitive amount of time.

The information which could be extracted from a powder pattern is not complete since the orientation of the field gradient components $V_{x'x'}$ and $V_{y'y'}$ with respect to the LAB remains unknown i.e. the angle α in Eqs. 2.15 and 2.16 could not be specified.

In order to get a better understanding of the severeness of the skin effect in a particular sample one can measure the magnetization in the x-y-plane as a function of the duration of the applied rf pulse, which is called the pulse width (pw).

A model for the skin effect in a sample in which the skin depth is much smaller than the sample size can be calculated. This case is equivalent to a metal; in the case of semiconductors it cannot be applied straightforwardly. The amplitude of a rf field in conducting materials decays exponentially with the distance from the surface with a skin depth δ as decay constant. The sample is assumed to be of semi-infinite volume, i.e. it has only one surface ($x = 0$). The sample is located in the right half space ($x \geq 0$). Using Eq. 2.6 one knows how the x, y-component of the magnetization produced by a spin i depends on the time t for which a rf pulse is applied

$$m_i(t) = m_0 \sin \phi_i = m_0 \sin \gamma B_1^i t.$$

But $m_i(t)$ really depends on the distance of the spin i from the surface since $B_1^i = B_1^i(x) = B_{surface} e^{-x^i/\delta}$. The field produced by the spin is again exponentially damped so that the total magnetization $M(t)$ in the transverse plane is proportional to the integral

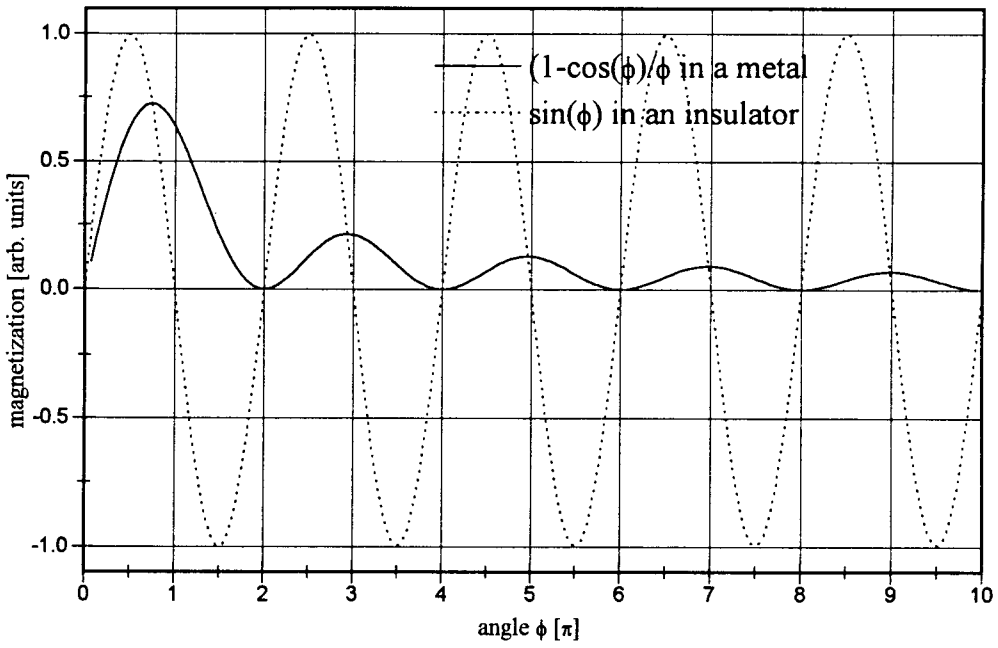

FIG. 3.3. Transverse Magnetization as a Function of Pulse Width

$$M(t) \sim \int_0^\infty dx e^{-\frac{x}{\delta}} \sin(e^{-\frac{x}{\delta}}\omega_1 t), \tag{3.2}$$

where $\omega_1 = \gamma B_{surface}$. This integral can be solved analytically by substitution of the argument of the sin-function in Eq. 3.2 and yields that the magnetization is proportional to

$$M(t) \sim \frac{\delta}{\phi(t)}\left(1 - \cos\phi(t)\right), \tag{3.3}$$

where $\phi = \omega_1 t$ is linear in the pw. The units will be correct if one introduces a magnetization density per unit length (m_0/L) in the conversion to the integral. A plot of Eq. 3.3 is shown in figure 3.3. It also shows the regular behavior of the magnetization in the x-y-plane as a function of the applied pulse width for the case of an insulator which is just a sin-function. It is clear that in case of very small skin depths much longer pulses are needed to invert the signal (2π versus $\frac{\pi}{2}$).

I have measured the transverse magnetization of ^{113}Cd in the samples 1,2,3 as a function of the applied pulse width. I used a pulse sequence in which the spin system was saturated initially, as described in the next section, and after a recovery time τ a pulse of different length (pw) was applied. The results are plotted in figure 3.4 and show that the model of very small skin depths does not accurately describe the case of highly doped semiconductors. The magnetization in my samples cannot be inverted at all. The gallium-doped sample 3 with the lowest number of free carriers exhibits the smallest skin effect, but the magnetization can still not be inverted. Sample 1 and 2 are indium doped, have a higher number of free carriers and show a stronger skin effect. It is interesting to notice that, although they are doped to different concentrations, their skin depth, i.e. their conductivity appears to be equal, which is in agreement with the data published by Watson and Shaw [6].

3.3.2. T_1 measurements

As shown in figure 3.4 the magnetization in the samples 1, 2, 3 cannot be inverted and therefore the use of the usual inversion recovery method to measure T_1 wouldn't work. Therefore all T_1 measurements were done using a saturation recovery method. This is a pulse sequence in which the spins are completely saturated by hundred pulses of $pw = 7.5\ \mu s$ with a time $\tau_1 = 1$ ms between the pulses. The pulse width is just that of a $\frac{\pi}{2}$-pulse in a non-conducting material. This causes an absolute equal population of the Zeeman levels by the spins, i.e. the spin temperature is infinite. After this comb of pulses one allows the spin system to recover for a time τ , i.e. to align in the magnetic field. One can measure the restored magnetization by applying another pulse of length pw at the end of the recovery time τ.

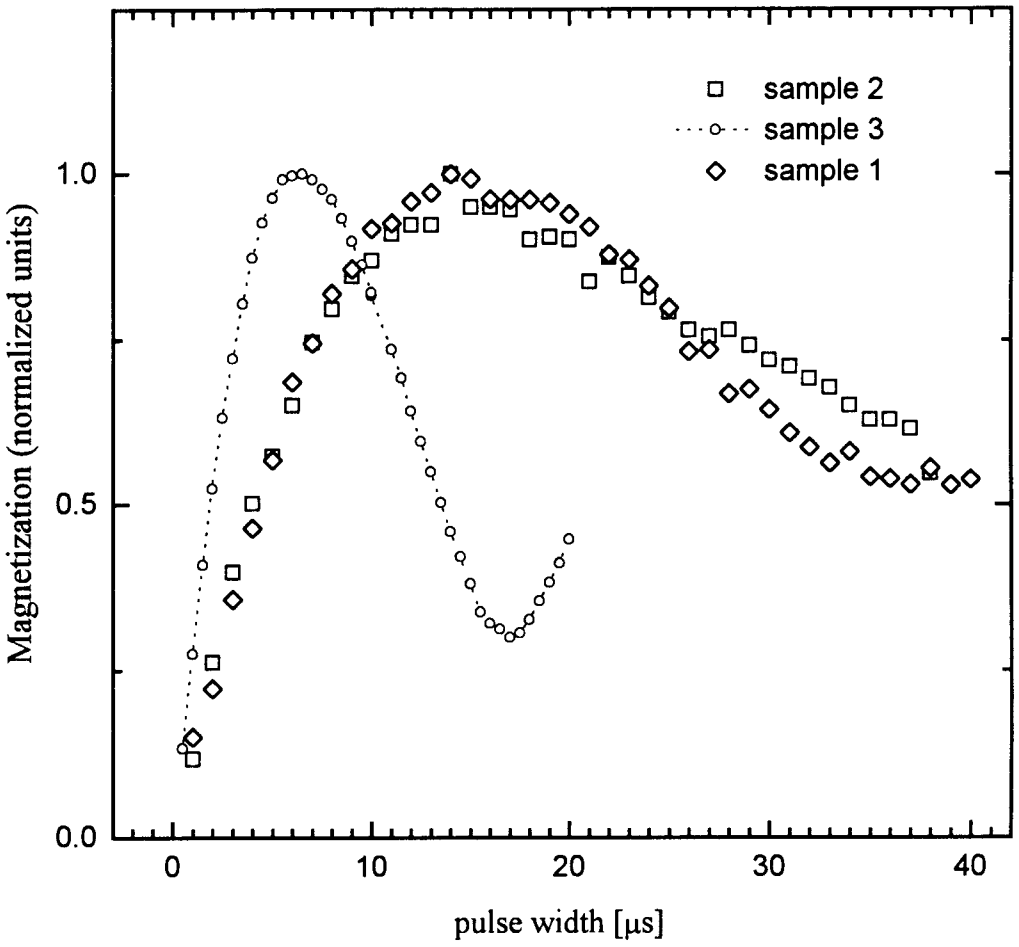

The magnetization has been measured in sample 1, 2, 3 using the saturation recovery method. The amplitudes were normalized. The ^{113}Cd resonance line in CdTe has a line width of at most 1 KHz, the spectrometer frequency was about 3 KHz off resonance, so that the pulse spectrum covers the whole line even for pw=40 μs

FIG. 3.4. Transverse Magnetization as a Function of Pulse Width in Sample 1,2,3

The advantage of the saturation recovery is that the spin system is prepared in the exact same state (saturation) for each measurement and one doesn't have to wait until the system is fully relaxed and in equilibrium with the lattice (at least five times T_1). For this reason even for the T_1 measurements on CdTe powder, where an inversion recovery sequence would be possible, the saturation recovery sequence is still the better choice. Since T_1 is very long ($T_1 \approx 400$ s at room temperature) the waiting period for the sample to equilibrate with the lattice would be very long and signal averaging not efficient.

The magnetization in a saturation recovery experiment ideally obeys the exponential relaxation

$$M(t) = M_0(1 - e^{-\frac{t}{T_1}}). \tag{3.4}$$

4. RESULTS AND DISCUSSION

4.1. SEARCH FOR THE INDIUM RESONANCE

Despite an extensive search for indium resonances in several samples I was not able to detect a signal which would be undoubtedly due to indium.

I started with a powdered sample of pieces of sample 2. FID's with very short pulses ($3 - 4$ μs) which would excite a broad frequency range in the sample were signal averaged for 1 million acquisitions, using a dwell time of 500 ns to ensure a wide spectral window to pick up resonances. The spectrometer frequency was altered from 74 MHz to 76 MHz in 500 kHz steps to look for resonances shifted upward in frequency due to coupling to conduction electrons (Knight-shift). I could not observe a resonance.

Since the doping level is low and a powder pattern might spread over a wide range I switched to a single crystal. The higher doped single crystal (sample 1) shows a skin effect similar to sample 2 and has a higher indium concentration. The crystal was oriented with its $\langle 100 \rangle$ axis along the $\overrightarrow{B_0}$ field. For nuclei experiencing an axial field gradient along the $\langle 111 \rangle$ direction of the crystal this should result in the collapsing of all satellite transitions onto one resonance line (see Eq. 2.15). Even if these favorable circumstances do not occur the central transition should still be detectable.

Using the single pulse sequence and a quadrupolar or solid echo sequence I did the same measurements as for the powder but could find no sharp resonance. This led to the conclusion that there isn't one well defined site on which all the

dopants experience the same environment and therefore the same resonance frequency.

In order to find out whether there is a wide distribution of resonance frequencies I altered the applied spectrometer frequency through a wide range. In case of a distribution one would always be on resonance and a Fourier transformation of the time signal would only show the spectral width of the probe circuit rather than the true resonance lines. Thus the time signal was used.

I scanned the time signals over a wide range of spectrometer frequencies using a quadrupolar echo sequence. In the time domain a weak echo could be seen and the integral of the signal was determined from 68 MHz to 96 MHz in 0.5 MHz steps. Each signal was averaged one hundred thousand times at a repetition rate of 33 Hz. The obtained spectrum couldn't be attributed to indium in the sample. It is possible that the echoes in the time domain are non-NMR effects due to ringing of the crystal caused by currents induced in the sample. The echo disappeared for dephasing times τ larger than 70 μs.

4.2. GALLIUM

4.2.1. Data on Gallium in a CdTe Single Crystal

Measurements on gallium in sample 3 are very time consuming, since the intensity of the resonance line is very weak. In order to find a resonance I looked for gallium in a doped CdTe powder first. Once I found the signal I switched to the crystal. To be sure the resonance line is due to gallium in the sample, I checked whether the second gallium isotope (^{71}Ga, $\nu_{res} \approx 103.875$ MHz in a 8 Tesla field) shows the expected resonance. Both isotopes showed the same shift with respect to the reference sample.

I then used larger and larger dwell times, which was only possible because the resonance line is very narrow. At large dwell times the spectrometer automatically selects narrow band filters which keep noise from outside the bandwidth from backfolding into the spectrum. This results in a better signal to noise ratio (s/n ratio) and shorter times are needed for signal averaging.

A very good spectrum of gallium in sample 3 is shown in figure 4.1, which shows the free induction decay of ^{69}Ga in sample 3. The FID was signal averaged 818032 times at a repetition rate of 1/(40 ms) so that the total measurement time was 10 hours. The temperature was reduced to $T = 213$ K to increase the signal strength. The s/n ratio is 40 calculated by taking the average of the noise on the baseline from -9 kHz to -2 kHz, multiplying it by $\frac{1}{\sqrt{2}}$ and divide the signal amplitude by this value.

The length of the acquired data set is 7.55×10^{-3}s, which are 151 points with a dwell time of $50\mu s$. The Fourier transformation was done using the raw data, so that the actual line width of the real part and the noise are shown. The zero on the time scale of the FID shown in figure 4.1 is located at a time $t_0 = 400$ μs after the end of the $\frac{\pi}{2}$-pulse. In order to display the long part of the FID on an acceptable intensity scale it is necessary to cut of the beginning of the FID. The large intensity right after the pulse is partly due to ringing, partly due to fast decaying components of the FID which will be discussed in the next section.

It can be seen that the envelope of the decay is not monotonic, but that there is a small beat frequency modulating the amplitude of the signal. This shows as two satellites left and right of the sharp resonance in the frequency domain. The spectrometer frequency is 81.718 MHz and the resonance is offset by $\nu_{sample} =$ (3.48$\pm$.04) kHz. The resonance shift δ is $-$(440$\pm$2) ppm with respect to the gallium chloride solution, where the shift is defined as $\delta = (v_{sample} - v_{reference})/v_{reference}$.

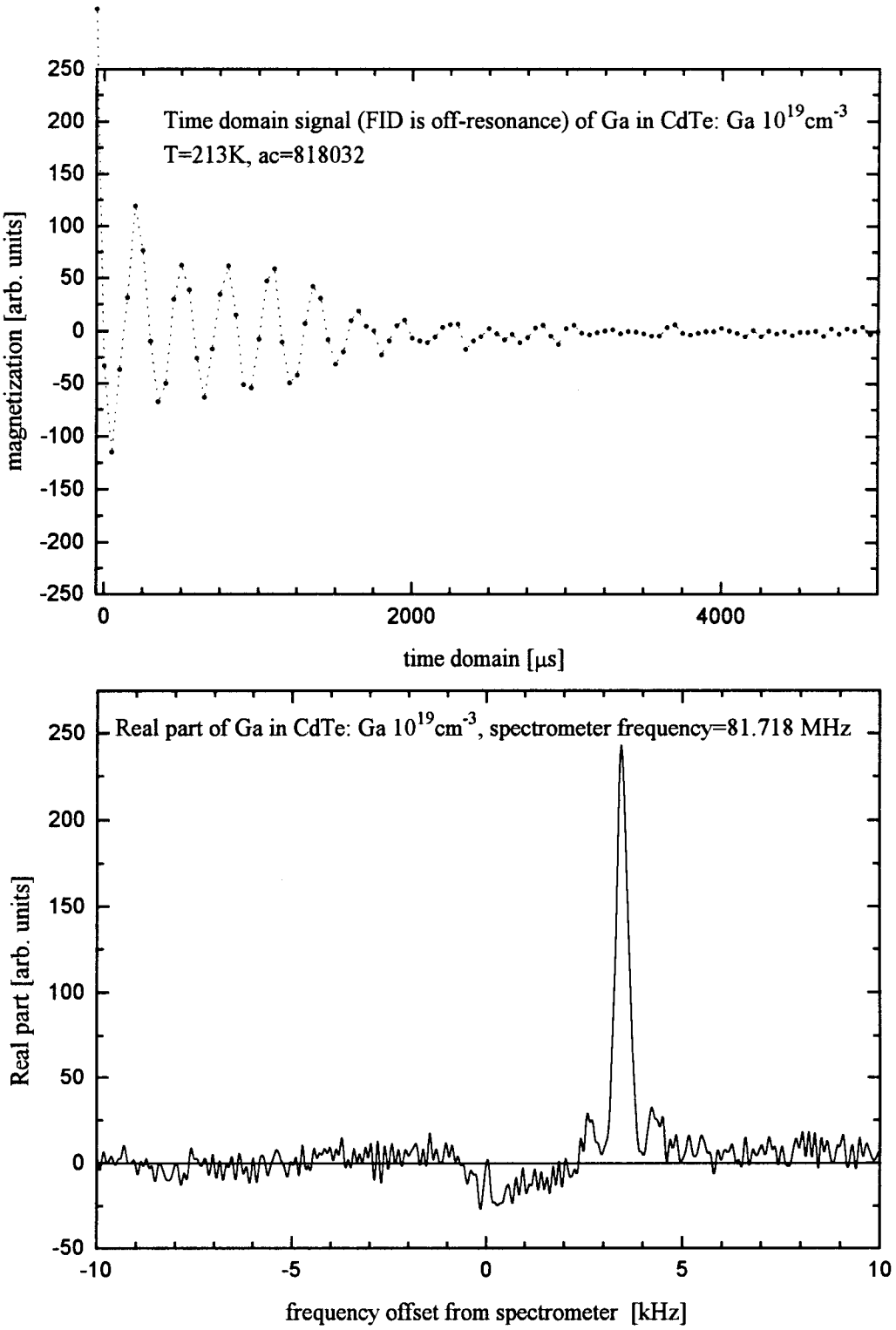

FIG. 4.1. FID and Spectrum of Gallium in Sample 3

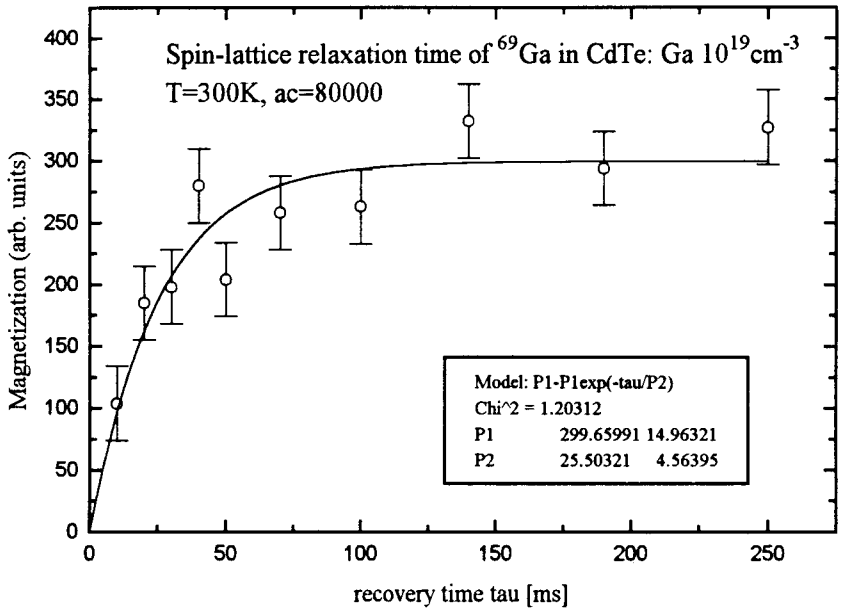

FIG. 4.2. Spin-Lattice Relaxation Time of Gallium

The shift δ doesn't change with temperature within $T = 213$ K and $T = 298$ K. The full width at half maximum of the line is $\Delta\nu = (0.35 \pm .05)$ kHz.

The splitting between the satellites is about $\nu_{split} = (1.7 \pm 0.1)$ kHz. The intensities and the positions of the satellites do not change, if the sample is rotated along the coil axis. It would be hard to improve the experimental error because an improvement of the s/n ratio would require at least two days for one measurement. I have measured the gallium resonance of the crystal at three different rotation angles $(0°, 45°, 105°)$. The relative intensities of the satellites compared to the central line are in the average $1 : (9.5 \pm 2) : 1$ for those three orientations.

T_1 measurements on gallium in sample 3 can not be very precise since the signal intensity is low. Using a saturation recovery sequence the spin-lattice relaxation time for ^{69}Ga was found to be $T_1 = (26 \pm 5)$ ms. The signal was acquired 80000 times for each recovery time τ. It took a total measurement time of $2\frac{1}{2}$ days at

isotope	T_1 [s]	shift [ppm]	line width [kHz]
^{69}Ga	26 ± 5	$-(440 \pm 5)$	$.35 \pm .05$
^{71}Ga	83 ± 13	$-(440 \pm 5)$	$.40 \pm .05$

TABLE I. Data on Gallium in Sample 3

room temperature to get the data which are plotted in figure 4.2. The error bars in the plot were determined by measuring the signal for a certain recovery time value ($\tau = 140$ ms) twice and taking two thirds of the difference as the error. In a similar measurement T_1 for the isotope ^{71}Ga was found to be $T_1 = (83 \pm 13)$ ms.

4.2.2. Interpretation

The spin-lattice relaxation times for the two gallium isotopes allow one to determine the dominant relaxation process. If the relaxation were mainly due to magnetic coupling of the nuclei to electrons, then the ratio of the relaxation rates should be about the square of the ratio of the gyromagnetic constants. This would mean

$$\frac{1/T_1\{^{69}Ga\}}{1/T_1\{^{71}Ga\}} = \left(\frac{10.22\frac{\text{MHz}}{\text{T}}}{12.984\frac{\text{MHz}}{\text{T}}}\right)^2 \approx 0.62.$$

In case of relaxation by coupling of the quadrupole moments of the nuclei to the electric field gradients, which vary in time due to thermal vibrations of the lattice, another ratio should be found. According to Mieher [21, p. 1544] the quadrupolar spin-lattice relaxation rate ($1/T_1$) in a zinc blende structure depends on the spin and the quadrupole moment of the nuclei in the following way

$$\frac{1}{T_1} \sim \left(\frac{2I+3}{40I^2(2I+1)}\right)(eQ)^2. \tag{4.1}$$

In case of the two gallium isotopes this yields the ratio

$$\frac{1/T_1\{^{69}Ga\}}{1/T_1\{^{71}Ga\}} = \left(\frac{0.178 \text{ barn}}{0.112 \text{ barn}}\right)^2 \approx 2.53.$$

The observed ratio of the measured relaxation rates is

$$\frac{T_1\{^{71}Ga\}}{T_1\{^{69}Ga\}} = \frac{(83 \pm 13) \text{ ms}}{(26 \pm 5) \text{ ms}} = 3.2 \pm 0.8$$

which includes the theoretical prediction for a quadrupolar relaxation process, while it differs substantially from the ratio predicted for magnetic coupling to the electrons. Therefore the dominant relaxation process must be quadrupolar in nature and even with the large error due to the low intensity a strong relaxation by coupling of the nuclei to conduction electrons can be excluded.

The relaxation rate of indium in CdTe can be estimated from Eq. 4.1. Taking the different spins and quadrupole moments into account the spin lattice relaxation time of ^{115}In is expected to be of the order of $T_1\{^{115}\text{In}\} \approx (7 \pm 2)$ ms. A saturation of the nuclei i.e. raising the temperature of the indium spin system to infinity can thus be excluded as an explanation for the lack of an indium resonance.

The satellites seen in figure 4.1 do not shift when the crystal is rotated around the coil axis suggesting that they may be due to an axially symmetric electrical field gradient at the site of the nuclei with its main component $V_{z'z'}$ coinciding with the coil axis. Eq. 2.15 would then reduce to $(\beta = \frac{\pi}{2}, \eta = 0)$ $\nu^{(1)} = \pm\frac{1}{2}\nu_Q$, where ν_Q is defined as $\nu_Q = (3e^2qQ)/(2Ih(2I-1))$. The coupling constant e^2qQ/h is equal to $(3.4 \pm .2)$ kHz. PAC publications report a much larger value of $\nu_Q \approx 60$ MHz. PAC is not sensitive enough to detect a field gradient in the kHz range.

The intensities of a quadrupolar split resonance line are proportional to the square of the transition matrix elements $|\langle m-1|I_-|m\rangle|^2 \sim I(I+1) - m(m-1)$. In case of ^{69}Ga $(I = \frac{3}{2})$ this yields a relative intensity of the satellites with respect

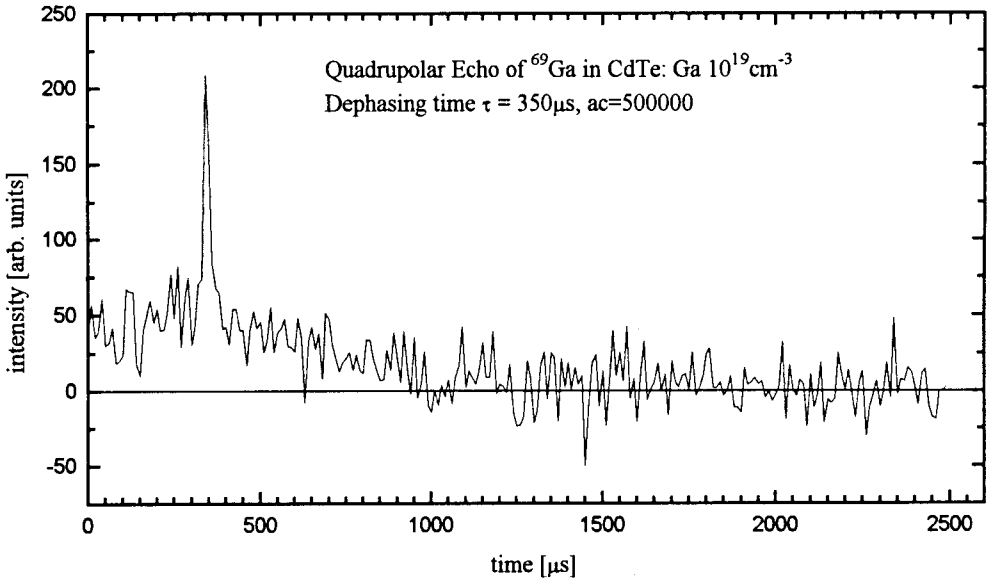

FIG. 4.3. Echo of Gallium in Sample 3

to the central transition of $1 : \frac{4}{3} : 1$. Taking the relative intensities of figure 4.1 into account a fraction of about 14% of the gallium nuclei experience this field gradient.

I have already mentioned that the FID in figure 4.1 has a huge intensity at the beginning of the data acquisition. It is not clear which part of it is ringing and to which extent it is due to a signal with a very short dephasing time constant T_2^*. Therefore I used a quadrupolar echo sequence, i.e. a sequence in which the magnetization is turned onto the $x-y$-plane by a $\frac{\pi}{2}$-pulse and after a time τ a second $\frac{\pi}{2}$-pulse with a phase shift of 90 degrees with respect to the first is applied. This sequence first described by Warren [25] for quadrupolar nuclei ($I \geq 1$) in solids, will refocus the spins at a time τ after the second pulse and an echo appears. I have measured an echo of ^{69}Ga in sample 3 for three different dephasing times $\tau = 250$, 300, 350, 800, 3500 μs in order to get a rough estimate of the spin-spin relaxation time T_2. The time domain signal with $\tau = 350$ μs is shown in figure 4.3. It was

gained by using a repetition rate of (1/50 ms) for 500000 acquisitions with a dwell time of 10 μs. An integration of the signal from $\tau - 20$ μs to $\tau + 20$ μs for the five sets gave values for the area underneath the signal of 4484, 3094, 3654, 2914, 1854 for the shortest to the longest τ value respectively. The error due to the poor resolution caused by the small digitization rate is about 400. Taking the natural logarithm of these values and using linear regression a value of $T_2 = (4.7 \pm 1.3)$ ms is found.

A comparison of the intensities of this broad frequency line to the line discussed previously is not possible, since it is not clear whether the narrow line is a selectively excited central transition, in which case the $\frac{\pi}{2}$-pulse condition would decrease [22]. Assuming the echo in the time domain has a full width of 30 μs at half height ($T_2^* = 15$ μs) and is a single exponential decay the line width in the frequency domain would be $\Delta\nu \approx 10$ kHz which can be easily picked up by the spectral range of the probe ($\approx .5$ MHz). The area underneath the time signal gets distributed over this 10 kHz range in the frequency domain and cannot be resolved with the present s/n ratio.

In conclusion one can say that an appreciable number of gallium nuclei in CdTe sit on sites of non-cubic symmetry. Those nuclei which contribute to the sharp echo in time domain (figure 4.3) probably sit on lattice sites which are only slightly distorted from their tetrahedral symmetry. This distortion is random in nature and therefore one gets a distribution in resonance frequencies of about 10 kHz line width. Another fraction sits on sites on which the nuclei experience an identical field gradient. Of the rest of the nuclei it is not clear if they experience an identical and large field gradient so that only the central line can be picked up or if they are located on sites without a field gradient.

4.3. CADMIUM

4.3.1. Relaxation Process and Line Width

4.3.1.1. Remarks on Hyperfine Coupling with Electrons

The contact term of the hyperfine coupling between a nucleus and an electron can be an important contribution to the internal Hamiltonian (Eq. 2.9) of a system. It is given by

$$H_{contact} = \frac{8\pi}{3}\gamma_e\gamma_n\hbar^2\sum_{j,l}\vec{I_j}\cdot\vec{S_l}\delta(\vec{r_l}-\vec{r_j}), \tag{4.2}$$

where $\vec{I_j}$ is the nuclear spin operator and $\vec{S_l}$ is the electron spin operator. The delta function expresses the fact that only electrons with a nonzero probability to be at the site of the nucleus can interact via direct spin-spin coupling. If the electron spins are polarized by the external field $\vec{B_0}$ the coupling will be nonvanishing and it will have a static component, which will give rise to a shift of the nuclear resonance frequency. Since the electron magnetic moment will be preferentially parallel to $\vec{B_0}$ the field at the site of the nucleus will be increased. Electrons obey the Pauli principle and thus only those in not completely filled shells can be polarized (paramagnetic impurities) and the extent to which they are polarized is given by a Curie law.

In case of a metal the electrons can be described as a noninteracting degenerate Fermi gas. They exhibit a Pauli paramagnetism (see e.g. Ashcroft and Mermin [23, p.661]) and their susceptibility is given by $\chi = \mu_B^2 g(\varepsilon_F)$ where μ_B is the Bohr magneton and $g(\varepsilon_F)$ is the density of states evaluated at the Fermi energy, i.e. in case of a metal, where the Fermi energy is constant over a wide range of temperature, the susceptibility due to the conduction electrons is constant too.

The Knight shift caused by the coupling of the nuclei to degenerate conduction electrons in metals is therefore independent of temperature as long as the temperature is small compared to the Fermi temperature.

Another characteristic of the contact interaction is that it does vary with time also. According to Heisenberg's Uncertainty principle the wave packet of an electron can not remain localized at the site of the nucleus for an indefinite time i.e. it will spread out in real space. Thus the nucleus is subject to a hyperfine field varying in time and thereby providing a relaxation mechanism for the nucleus. In this relaxation process the nucleus gives the energy ε_N released by its own spin flip in the magnetic field to a conduction electron. The conduction electrons obey Fermi statistics, their average energy is much bigger than kT and is of the order of the Fermi energy ε_F, but because of the Pauli principle only a fraction of them is able to pick up the energy ε_N released by the nuclei. This fraction are those electrons in $\overrightarrow{k}$-space which are close enough to the Fermi surface to be scattered into an empty state $\overrightarrow{kl}$ above the Fermi surface by the contact interaction. Their number is proportional to kT and so is the nuclear relaxation rate $1/T_1$.

Both the nuclear relaxation rate $1/T_1$ and the Knight shift involve the probability density of an electron to be located at the site of the nucleus. They can be related by this feature and the so called Korringa relation can be established

$$T \cdot T_1 \cdot \left(\frac{\Delta H}{H_0}\right)^2 = \frac{\hbar}{4\pi k}\left(\frac{\gamma_e}{\gamma_N}\right)^2, \tag{4.3}$$

where the product of the temperature T , the relaxation time T_1 and the square of the Knight shift is constant.

In case of semiconductors one has to take into account that the electrons do not longer obey a Fermi-Dirac statistic but they are distributed on the states in the conduction band according to a Boltzmann distribution. The density of

electrons in the conduction band is small and the electron gas is non-degenerate. The density of states available to the electrons is now temperature dependent and a calculation of the relaxation rate $1/T_1$ yields [24], [16, ch.IX] that the relaxation rate is proportional to the square root of the temperature ($\frac{1}{T_1} \sim \sqrt{T}$).

4.3.1.2. Line Widths in a Zinc Blende Crystal

The resonance line of a nuclear species in a magnetic field can be broadened by two principally different processes. The line is called inhomogeneously broadened if the spins of one species sit on non-identical sites e.g. if there is a distribution of field gradients in a crystal, the field gradient the individual nucleus is subjected to will vary in a random fashion or if the sample sits in an inhomogeneous magnetic field. The line is called homogeneously broadened if the line width is due to interactions among the spins.

The homogeneous broadening due to interaction among the spins is of interest here. A spin 1 in the external field $\overrightarrow{B_0}$ will rotate around the field and thus produce a local static field at the site of spin 2. The orientation of the static local field depends on the relative orientation of the two spins. Since there are many spins in the sample there will be a distribution of local fields and a line broadening. Spin 1 will also produce a component rotating in the $x-y$-plane at the site of spin 2 and thus the spin 2 experiences a static field in its own rotating frame if this component is on resonance with the Larmor frequency of spin 2. This can change the orientation of spin 2 and contribute to the line width. In case of unlike spins the rotating component of the dipolar fields will be off resonance and not be effective.

A derivation of the line width due to dipolar broadening is given in both Abragam [16, ch.IV] and Slichter [12, ch.3]. The second moment of a line broadened by like spins is about the square of the line width and given by

$$M_2^{like} = \overline{\Delta\omega^2} = \frac{3}{4}\gamma_N^4\hbar^2 I(I+1)\sum_k \frac{(1-3\cos^2\Theta_{jk})^2}{r_{jk}^6}, \tag{4.4}$$

where Θ_{jk} is the angle between the line connecting the spin j, whose line is broadened by all the other spins k, and the magnetic field $\overrightarrow{B_0}$.

The second moment of a line broadened by unlike spins is given by

$$M_2^{unlike} = \overline{\Delta\omega^2} = \frac{1}{3}\gamma_I^2\gamma_S^2\hbar^2 S(S+1)\sum_{k'} \frac{(1-3\cos^2\Theta_{jk'})^2}{r_{jk'}^6}, \tag{4.5}$$

where the summation goes over all spins $S_{k'}$ surrounding spin I_j. The line width depends on the crystal structure and on the interatomic distances in the crystal and on the orientation of the crystal in the field. This influence is summed up in the so called lattice sum.

I calculated this sum for 149 nuclei surrounding a ^{113}Cd nucleus in sample 3 for a case in which the $\langle 100\rangle$ axis is parallel to the magnetic field $\overrightarrow{B_0}$. The line width in the indium doped samples should be very close, since the magnetic moments of indium and gallium are similar. It is not clear how large the error made by cutting off the sum after a number of terms is, but the terms for the nuclei farthest out were by a factor of 10^{-3} smaller than the first term in the sum so that this calculation yields at least the correct order of magnitude. The two cadmium isotopes were assumed to have the same magnetic moment and their abundance was added to a total of 25%. The two gallium isotopes were taken into account individually, while only ^{125}Te entered the calculation since the other isotopes are in low abundance. The line width is gained by adding the second moments 4.4, 4.5 and taking the square root afterwards and found to be

$$\Delta\nu = \frac{\Delta\omega}{2\pi} \approx 72 \text{ Hz}.$$

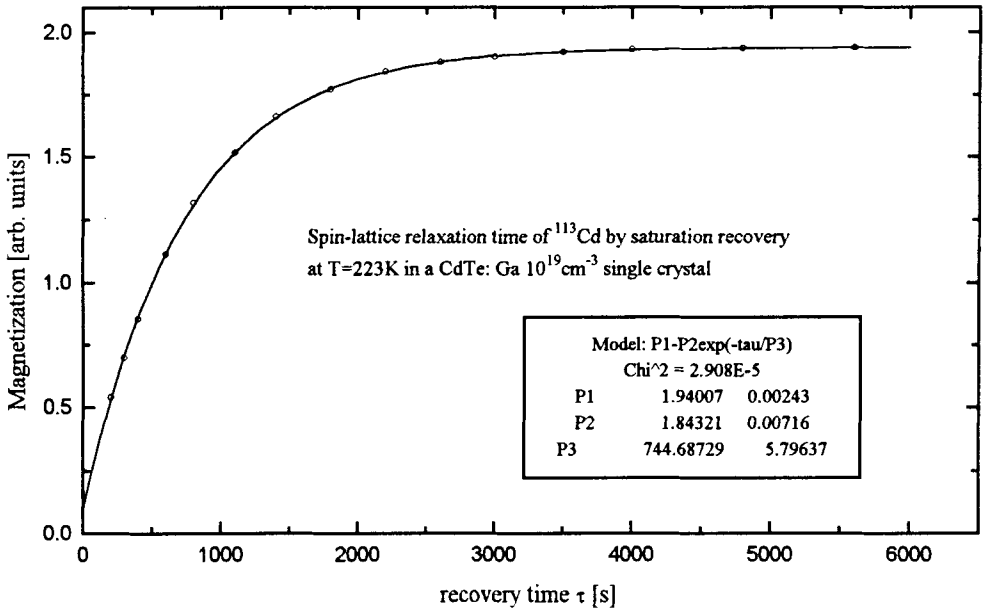

FIG. 4.4. Spin-Lattice Relaxation Time of Cadmium in Sample 3

4.3.2. Data on Cadmium in Sample 3

The spin-lattice relaxation time T_1, the shift with respect to a reference sample and the line width of ^{113}Cd in a (CdTe: Ga 10^{19}cm^{-3}) single crystal were measured in the temperature range from T = 153 K to T = 423 K. All the T_1 measurements were done using a saturation recovery sequence with 100 pulses of 7.5 μs duration and one millisecond apart to saturate the sample. The magnetization which was restored after a recovery time τ was measured with another pulse of 7.5 μs. I did not use signal averaging since the relaxation time is long and the huge signal of the host species allows to achieve a good s/n ratio with only one acquisition. A T_1 measurement is shown in figure 4.4, which was done at T = 223 K. The error for T_1 is assumed to be between 1% and 9% depending on the quality of the measurement, i.e. on the s/n ratio and on how many points on the base line were measured. The fit in figure 4.4 yields a value of T_1 = 747 s of which the error is assumed to still

T [K]	T_1 [s]	shift [ppm]	line width [kHz]
153	1196 ± 60	293.1	$.37 \pm .01$
223	747 ± 7.5	285.5	$.38 \pm .01$
273	500 ± 10	279.5	$.37 \pm .01$
323	454 ± 9	273.3	$.37 \pm .01$
373	356 ± 11	266.8	$.35 \pm .01$
423	310 ± 30	-	-

TABLE II. Data on ^{113}Cd in Sample 3

be 1%. If one wants to get a better understanding of the error one would need to measure T_1 several times but this would take a long time since about 10 hours are needed for one value. The data on the shifts and line widths were taken from these measurements. All the data are listed in table II.

The spin-lattice relaxation rate $1/T_1$ divided by the temperature and the shift and line width at different temperatures are shown in figure 4.5. $1/(T_1T)$ seems to be constant at $(7.5 \pm .2) \times 10^{-6} \frac{1}{\mathrm{sK}}$ for temperatures between 273 K and 423 K.

Using the Korringa relation 4.3 and $(7.5 \pm .2) \times 10^{-6} \frac{1}{\mathrm{sK}}$ for $1/(T_1T)$ one can calculate a value for the Knight shift if the relaxation is due to coupling to degenerate conduction electrons as suggested by the constant value of $1/(T_1T)$. Then the Knight shift would be constant at $\delta_{knight} = (6.3 \pm .2)$ ppm.

Therefore the main part of the shift must be due to some chemical shift, the total shift can be described by

$$\delta(T) = 312\mathrm{ppm} - 0.12\frac{\mathrm{ppm}}{\mathrm{K}}T$$

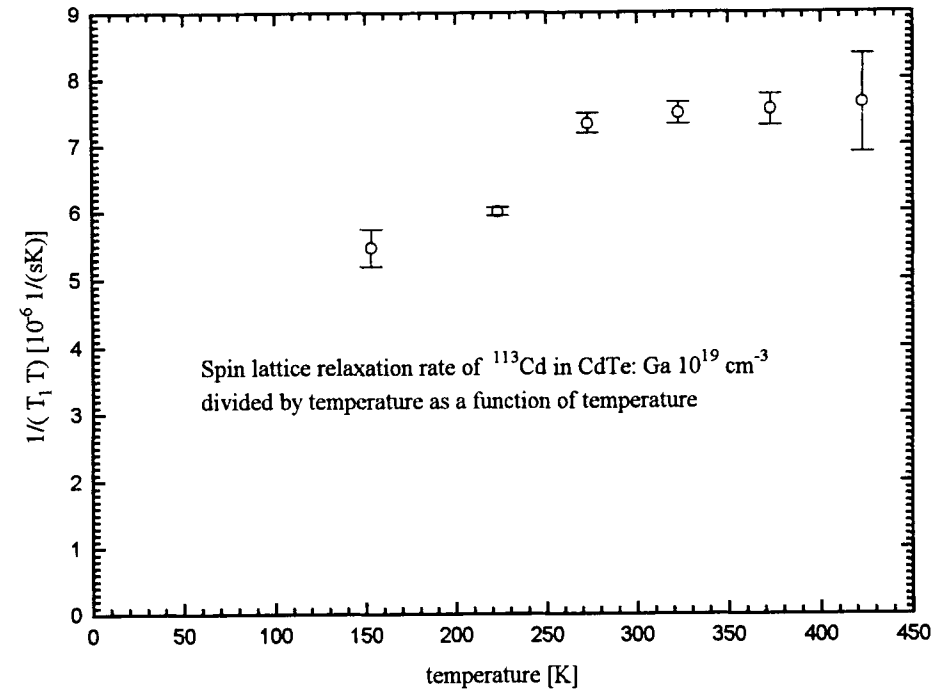

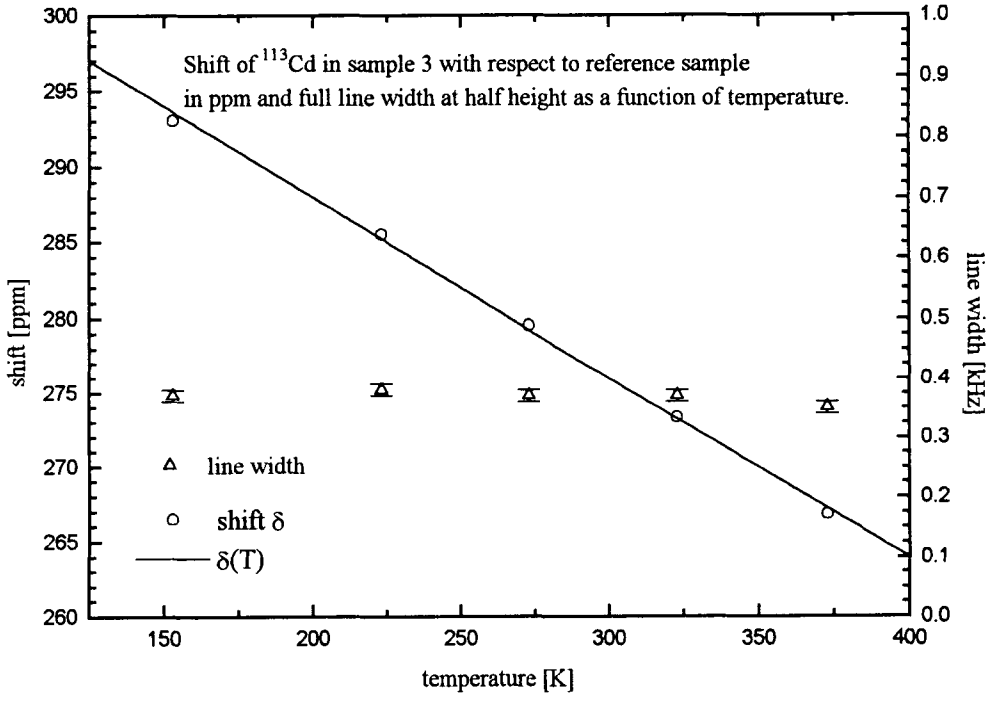

FIG. 4.5. Relaxation Rate, Shift and Line Width of Cadmium in Sample 3

T [K]	$T_1[s]$	shift [ppm]	line width [kHz]
218	800 ± 32	287.1	$1.10 \pm .04$
273	583 ± 23	278.1	$1.12 \pm .04$
323	401 ± 20	271.5	$1.10 \pm .04$
423	265 ± 11	257.8	$0.88 \pm .05$
493	212 ± 6.4	249.6	$0.80 \pm .04$

TABLE III. Data on ^{113}Cd in Sample 4

within the plotted temperature range. The shift depends linearly on the temperature and the dependence on the doping level and the kind of dopant is negligible as will be discussed later.

The line width is constant within the experimental error and within this temperature range. Its value is by a factor of 5 larger than expected from the calculation of the dipolar contribution to the line width. A line width of 350 Hz corresponds to about 5 ppm and is thus a variation of about 1.7% of the chemical shift only. This could be caused by random strains in the material.

4.3.3. Data on Cadmium in Sample 4

Similar measurements as on the doped sample 3 were done on sample 4 which is a commercially available undoped powder of CdTe. Depending on the temperature 4 to 6 acquisitions were necessary to achieve a good s/n ratio in the T_1 measurements, which were done using a saturation recovery sequence. The data on T_1, the shift and the line width at different temperatures are listed in table III.

The values calculated for $1/(T_1T)$ and $1/(T_1\sqrt{T})$ as well as the line width and the shift are shown in figure 4.6.

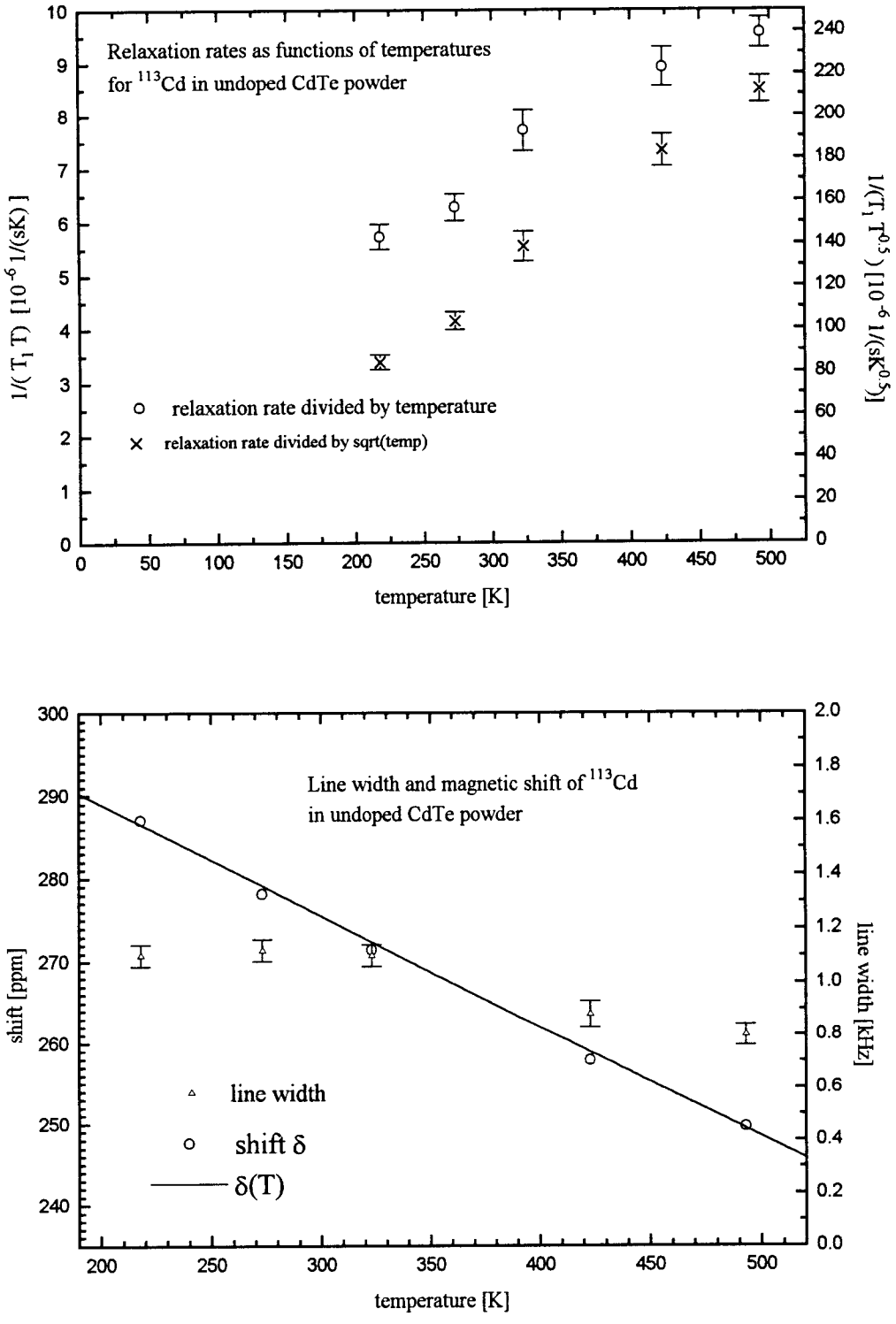

FIG. 4.6. Relaxation Rate, Shift and Line Width of Cadmium in Sample 4

The relaxation rate $1/T_1$ is plotted in two different ways: once it is divided by the temperature T and once it is divided by the square root of the temperature $\sqrt{T}$. Neither of those sets is constant over a temperature range, indicating that the relaxation can't be described by coupling to a constant concentration of degenerate or non-degenerate conduction electrons. $1/(T_1T)$ keeps increasing with temperature and actually rises above the value found in the highly doped sample 3.

The shift can again be described by a linear function

$$\delta(T) = 316\text{ppm} - 0.135\frac{\text{ppm}}{\text{K}}T,$$

and taking the error into account this is very similar to the temperature dependence of the shift $\delta(T)$ of ^{113}Cd in sample 3.

4.3.4. Data on Cadmium in Sample 2

Sample 2 is an indium doped cadmium telluride single crystal (CdTe: In $1\times10^{19}\text{cm}^{-3}$). The spin-lattice relaxation time T_1 for ^{113}Cd was measured at $T = 223$ K. A saturation recovery sequence with different recovery times τ was used; the number of acquisitions is between 2000 and 400; the total measurement time was 36 h. It is necessary to use two exponentials to fit the relaxation curve (figure 4.7), which means that there are at least two distinct sites of cadmium whose coupling of the cadmium nuclei to the lattice is different. A plot of a spectrum acquired with a saturation recovery sequence and a recovery time $\tau = 1$ s averaged 20000 times is shown in the same figure and shows at least 4 distinct components. The zero on the frequency scale corresponds to a zero offset from the spectrometer frequency which is in this case equal to 75.7 MHz. The spectrum in figure 4.7 depends strongly on the recovery time τ because the spins on different sites have different relaxation times T_1, so that for short recovery times the fast relaxing spins contribute strongly

peak	offset [kHz]	shift [ppm]	T_1 [s]	amplitude
peak 4	$-(1.8 \pm .1)$	238.6	-	-
peak 3	$-(0.7 \pm .1)$	253.2	2.6 ± 1	2.8 ± 1
peak 2	$+(0.32 \pm .05)$	266.7	3.8 ± 1.5	3.8 ± 2
peak 1	$+(1.16 \pm .05)$	277.8	7 ± 4	12 ± 8

TABLE IV. Data on ^{113}Cd in Sample 2

whereas the slowly relaxing spins are still partially saturated at the time of the $\frac{\pi}{2}$-pulse and their magnetization along the z-axis is weak.

The peaks from negative to positive frequencies are shown in table IV. The error in the shift is small i.e. in the worst case of the order of 1 ppm. The line width is larger than in sample 3, it is about 700 Hz but still only 3.5% of the chemical shift. It is very interesting that peak 1,2,3 which have different shifts also have different relaxation times T_1. A rough estimate on the values for the T_1's of the different sites can be gained by integrating the spectra for the different τ values in a small band of ± 0.2 kHz around the peak offset given in table IV. Peak 4 is not resolved in the spectra of the T_1-measurement, since the s/n ratio is poor compared to the spectra in figure 4.7 and no value for T_1 was extracted. The values for the spin-lattice relaxation times T_1 for the three other peaks are given in the table, they were determined by fitting the values of the integrals to a single exponential. The amplitudes in the table are the amplitudes of the fit. The T_1-values are not very accurate, i.e. they have large error limits, but a definite trend can be seen i.e. the smaller the shift with respect to the reference the shorter is the spin-lattice relaxation time. This may be explained by a non-uniform density of conduction electrons throughout the sample causing the nuclei to relax faster in areas of higher densities, since the shift should

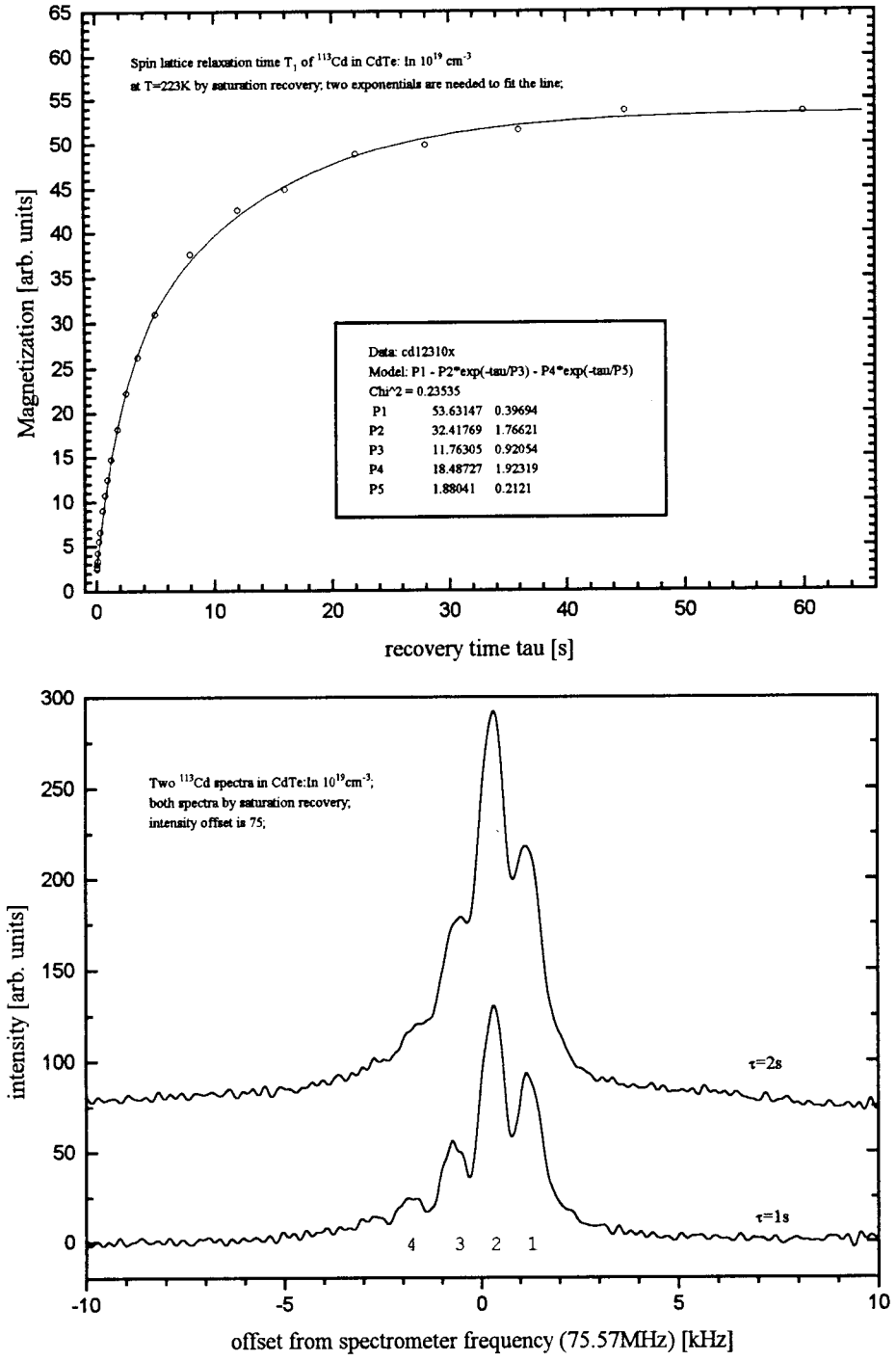

FIG. 4.7. Relaxation Curve and Spectra of Cadmium in Sample 2

decrease in those regions, i.e. have less paramagnetic values for nuclei in areas with a high conduction electron density instead of more paramagnetic values. The effective g factor g^* is reported to be negative and thus cause negative, diamagnetic Knight shifts. The overall effect of a substantial decrease of the spin-lattice relaxation time T_1 is expected, since the number of free carriers in sample 2 is two orders of magnitude higher than in sample 3.

The two spectra in figure 4.7 are from similar measurements. The recovery time τ is different in the two spectra and one can see the influence of the different relaxation times T_1 in the spectrum i.e. the ratios between the areas underneath the peaks have changed. The crystal was also rotated around its growth axis and the position of the peaks in the frequency domain remains the same i.e. the shift is isotropic and thus an interaction which depends on the orientation of the crystal in the field as an explanation for the splitting seems unlikely.

The temperature dependence of the shift of ^{113}Cd was measured less accurately than for the previous samples i.e. the s/n ratio was not good enough to resolve the individual peaks but the change of the shift with temperature of $\Delta\delta/\Delta T = -(0.1 \pm 0.03)\frac{\text{ppm}}{\text{K}}$ is close to the values found in the other samples.

4.3.5. Data on Cadmium in Sample 1

Sample 1 is a single crystal of cadmium telluride doped with indium to one atomic percent (CdTe: In $1.5 \times 10^{20}\text{cm}^{-3}$) and is cut along the $\langle 100 \rangle$ axes. The spin-lattice relaxation time T_1 in sample 1 was measured by saturation recovery at a temperature $T = 248$ K with the external magnetic field $\overrightarrow{B_0}$ along the $\langle 111 \rangle$ axis of the crystal. The data are shown in figure 4.8. As in the case of sample 2, it can not be fitted to one single exponential (dotted line), while a two exponential

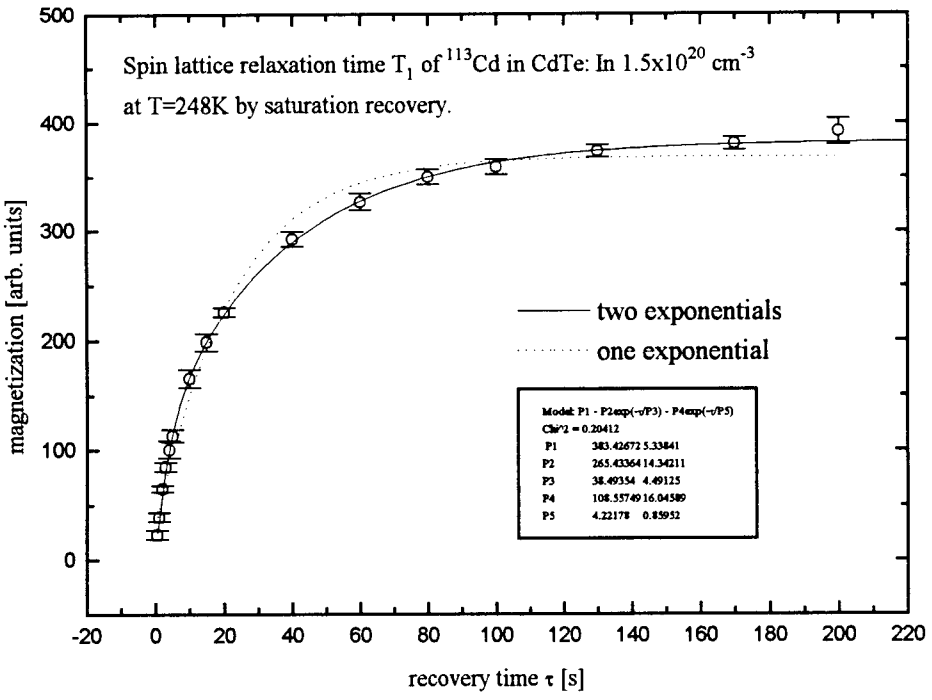

FIG. 4.8. Relaxation Curve of Cadmium in Sample 1

model (full line) allows a reasonable fit. This indicates that there are at least two sites with different spin-lattice relaxation times T_1, the longer of which is about $T_1 = (38 \pm 5)$ s. This is much shorter than the relaxation times in the undoped powder sample or in the gallium doped sample and can be explained by the higher carrier concentration. As mentioned before the free carrier concentration in sample 1 is comparable with the one in sample 2 (see also [6, figure 8]), so that both samples should have similar relaxation times. However there is a factor of 3-4 difference between the relaxation times of sample 1 and sample 2. The T_1 measurements were done at different temperatures and since the temperature dependence of the spin-lattice relaxation time in the indium doped samples is not known, it is not possible to compare the two values.

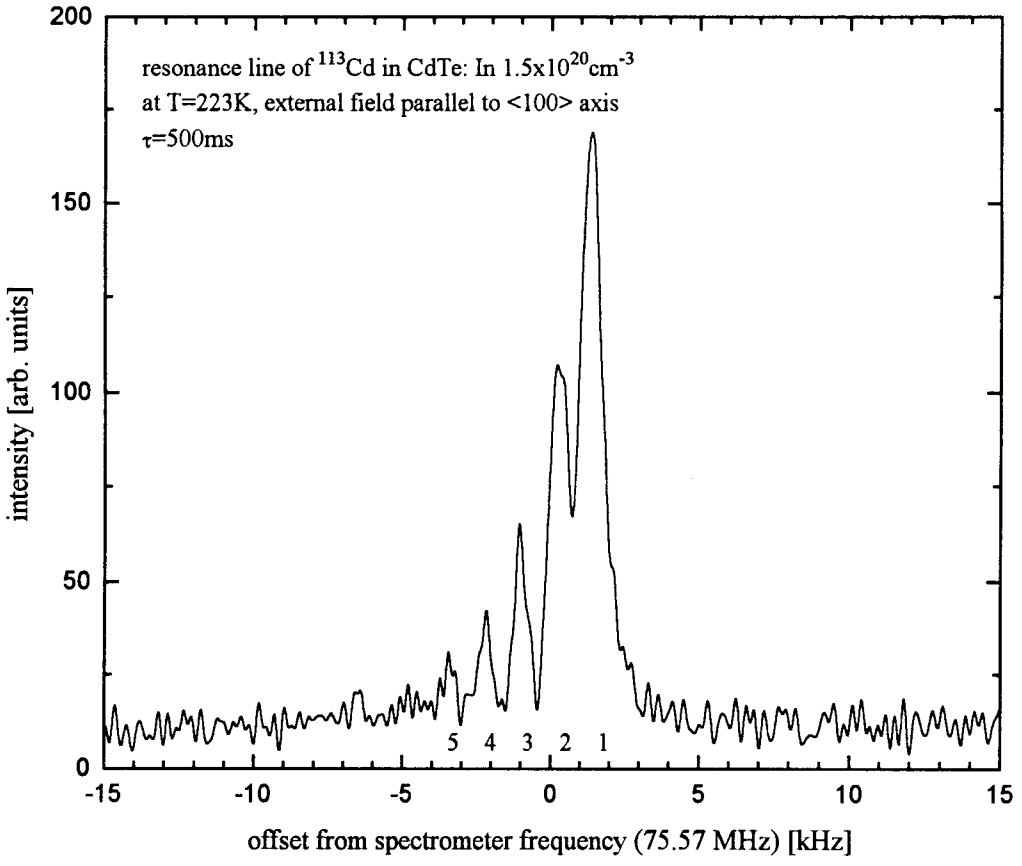

FIG. 4.9. Spectrum of Cadmium in Sample 1

A spectrum of ^{113}Cd is shown in figure 4.9. It was gained by saturation recovery with a recovery time $\tau = 500ms$ at a temperature of $T = 223$ K and was averaged 118420 times. The crystal was oriented so that a $\langle 100 \rangle$ axis was parallel to the external magnetic field. The ^{113}Cd resonance is split into 5 lines: a dominant line and four lines which are less intense and shifted to lower frequency or lower local field. The resonance frequencies of the individual peaks do not depend on the orientation of the crystal axes with respect to the magnetic field. Similar measurement as the one shown in figure 4.9 were done for three different orientations of the crystal, i.e. the $\langle 100 \rangle, \langle 110 \rangle, \langle 111 \rangle$ axes were aligned parallel to the external magnetic field. The spectra matched within the experimental error.

peak	offset [kHz]	line width [kHz]	shift [ppm]
peak 1	1.32 ± 0.1	1.0 ± 0.1	279 ± 2
peak 2	0.25 ± 0.1	1.0 ± 0.1	265 ± 2
peak 3	-1.0 ± 0.1	0.8 ± 0.1	248 ± 2
peak 4	-2.2 ± 0.1	-	232 ± 2
peak 5	-3.45 ± 0.1	-	216 ± 2

TABLE V. Data on ^{113}Cd in Sample 1

The data of the resonance frequencies of the individual peaks and their shift $\delta = (\nu_{res} - \nu_{ref})/\nu_{ref}$ with respect to a reference sample (0.1 molar solution of $CdSO_4$, $\nu_{ref} = (75.55024 \pm 0.00002)$ MHz) are listed in table V. The line widths for peak 4 and peak 5 were not listed, since the error is too big. The line widths of peak 1, 2, 3 are larger than in sample 2 or in sample 3 and are of the size of the line width of ^{113}Cd in the powdered sample.

As already seen in sample 2 the relaxation times of the peaks are different. The peaks 2, 3, 4 have a shorter spin-lattice relaxation time T_1 than the dominant line, which can be seen in figure 4.10. Peak 5 is not resolved since the measurement was done at higher temperature so that the Curie magnetization is smaller and the signal was averaged 50000 times only. The spectra shown in figure 4.10 are measured by saturation recovery, where the recovery time τ is the time for which the spins are allowed to relax after the initial saturation. The data were gained at $T = 248$ K with the external field along the $\langle 111 \rangle$ direction of the crystal. The relative intensities of the peaks change and for short recovery periods τ peak 1 gets saturated the most and its intensity drops below the intensity of peak 2. Peak 4 and 3 relax very fast,

while peak 2 gains quite some intensity from $\tau = 100$ ms to $\tau = 300$ ms but doesn't increase further from $\tau = 300$ ms to $\tau = 400$ ms.

Another plot of spectra gained for different recovery times ($\tau = 1, 2, 3$ s) is shown in figure 4.11. The spectra show how peak 1 grows to a very intense line if it is allowed to relax longer. The structure of the line gets washed out or swallowed by the intense line. The spectra were gained by saturation recovery at $T = 223$ K and $\vec{B_0}$ along the $\langle 100 \rangle$ axis. They were averaged 10000 times for $\tau = 1, 2$ s and 5000 times for $\tau = 3$ s. They are displayed with correct relative intensities, i.e. the spectrum with $\tau = 3$ s was multiplied by two. Therefore the noise level in this spectrum ($\tau = 3$ s) is not as low as in the other two spectra ($\tau = 1, 2$ s) as can be seen in figure 4.11.

It is interesting to compare the spectra of ^{113}Cd for the two limiting cases: the first case in which the intense peak 1 is saturated and the line structure can be resolved and the second case in which the nuclei are allowed to fully relax and therefore peak 1 dominates. The two spectra shown in figure 4.12 allow this comparison. The upper spectrum gained with a recovery time $\tau = 200$ s was averaged 100 times and multiplied by a factor of 30 in the plot. The lower spectrum for the shorter recovery time was acquired 92224 times. For a comparison of the two lines one has to realize that the upper spectrum would have to be multiplied by an additional factor of 31 to be able to compare the amplitudes of the spectra. The noise on the baseline has the correct size since it is already multiplied by a factor of 30 which is about the square root of the ratio of acquisitions between the spectra (noise adds proportionally to the square root of the number of acquisitions). As we already saw in figure 4.10 the peaks 2, 3, 4, 5 have mostly relaxed after a recovery time $\tau = 500$ ms, so that in comparing the spectra in figure 4.12 it becomes clear why the peaks

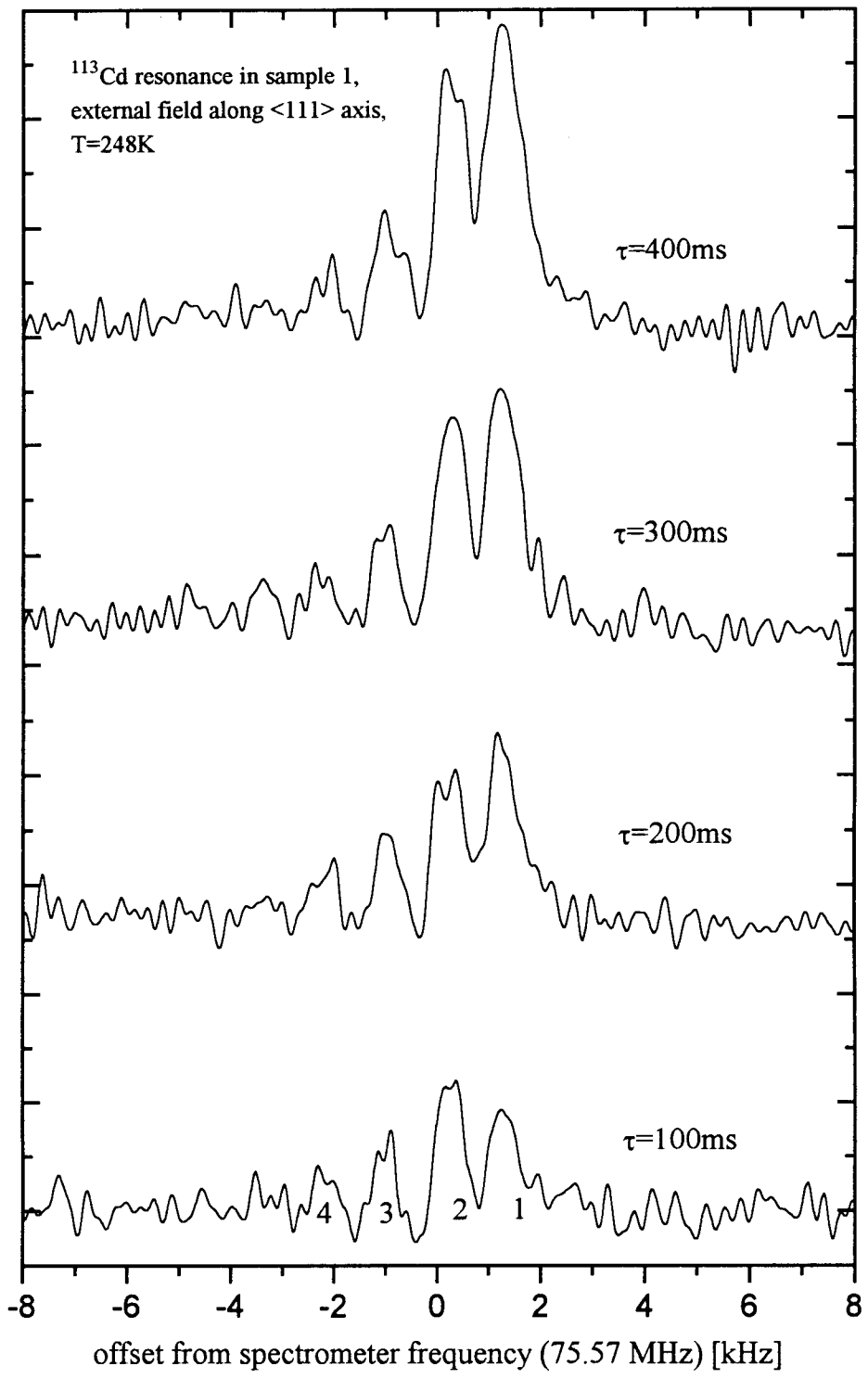

FIG. 4.10. Spectra of Cadmium in Sample 1 and short Recovery Times

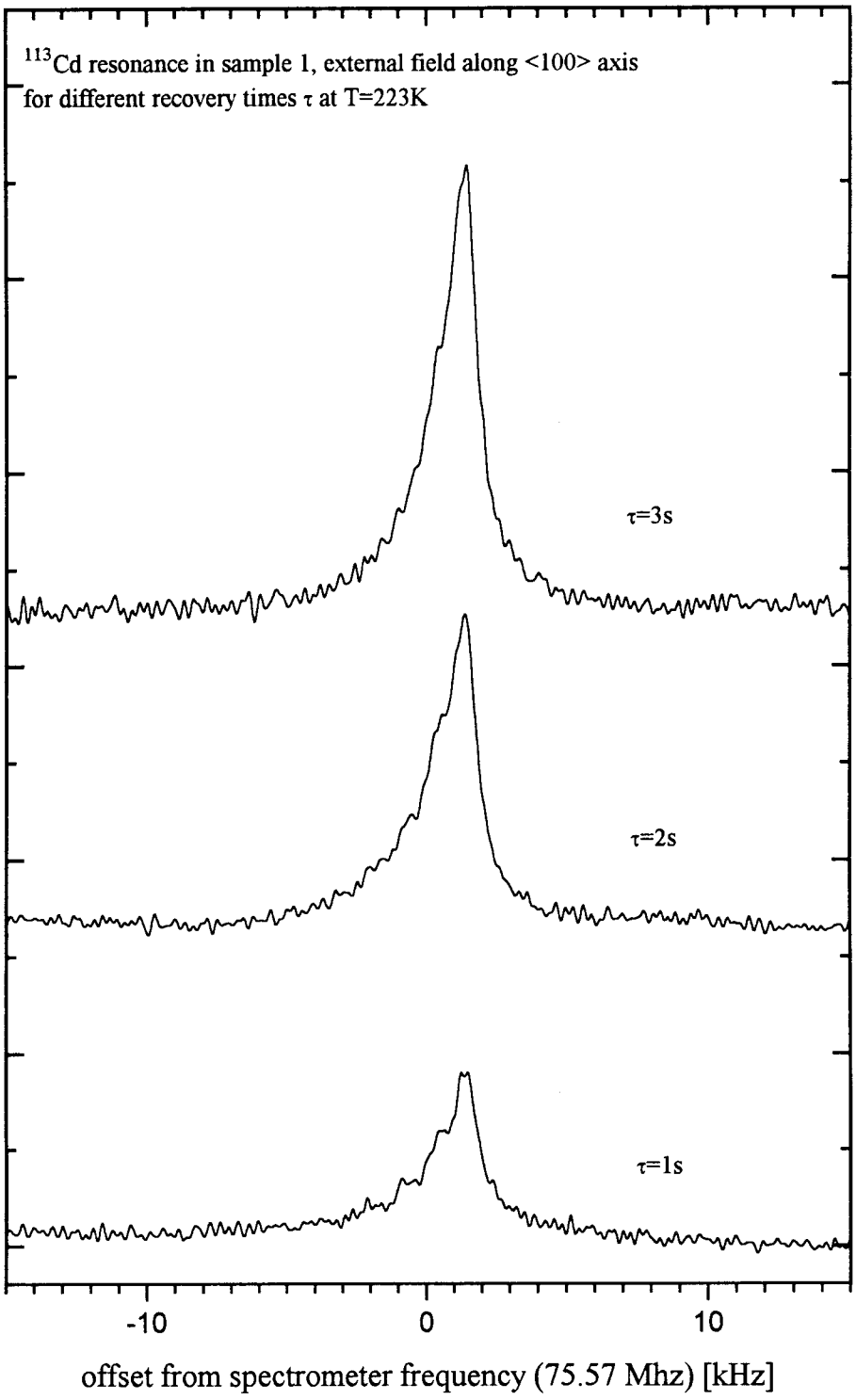

FIG. 4.11. Spectra of Cadmium in Sample 1 and longer Recovery Times

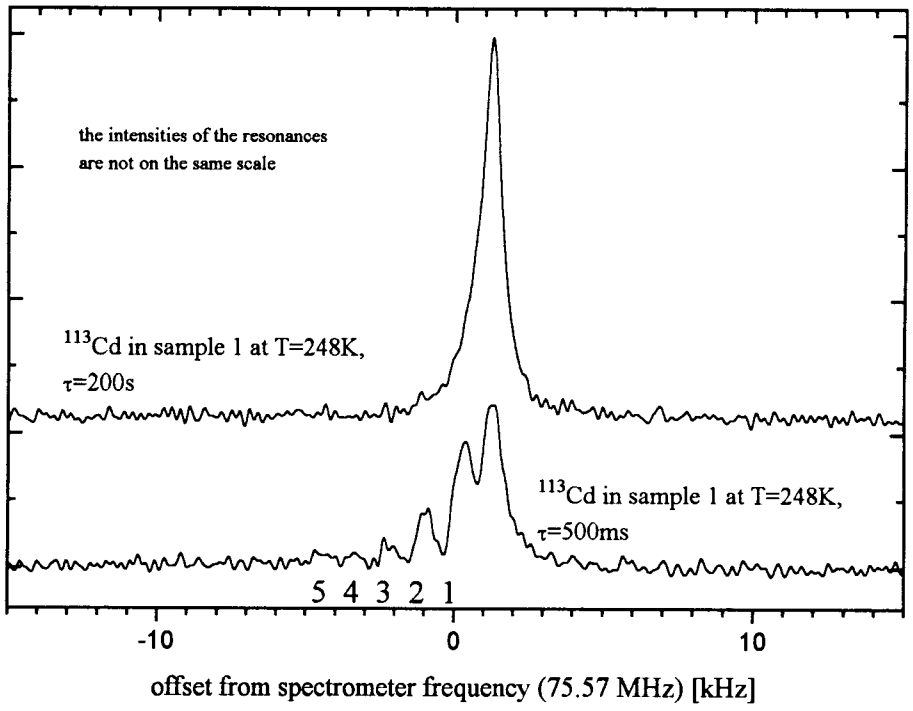

FIG. 4.12. Fully relaxed Spectrum of Cadmium in Sample 1

2, 3, 4, 5 are not resolved in the fully relaxed spectrum. One is looking for signals of the intensity of the lower spectrum on the scale of thirty times the upper spectrum.

A quantitative analysis of the relative intensities can be done in the following way: the integral over the peaks 2-5 in the lower spectrum in figure 4.12 i.e. from $\nu = -3.6$ kHz to $\nu = 0.65$ kHz can be compared to the intensity of the whole upper spectrum ($\tau = 200$ s). Taking the different number of acquisitions into account one finds that the integral of the peaks 2-5 is 1.1% of the total intensity of a fully relaxed line. Although the error is large and probably up to a factor of two, the fraction of cadmium atoms, which contribute to the peaks 2-5, is of the same order as the fraction of indium dopants in the crystal, which is doped to one percent.

4.3.6. Data on Cadmium in Sample 5

The primary task of the NMR measurements on this sample was to check whether the splitting of the ^{113}Cd resonance line in the indium doped samples is due to the dopant or is a property of cadmium telluride single crystals. The sample was provided by the same source and grown by the same technique, so that the only apparent difference is that samples 1, 2 are indium doped and sample 5 is a pure crystal.

The spin-lattice relaxation time of sample 5 was not measured but it is expected to be close to the value found in undoped powder of CdTe (sample 4) and be about $T_1 = 450$ s at room temperature. The pulse width condition for a $\frac{\pi}{2}$-pulse was measured and found to be 7 μs as expected for a material in which the skin depth is larger than the sample size. The magnetization could be inverted with a pulse width of 16 μs and the magnetization turned onto the x-y-plane depends sinusoidally on the pulse width, i.e. problems due to a skin effect do not arise in this material.

In order to try to find structure which might have a small intensity and be due to fast relaxing cadmium nuclei, I measured the ^{113}Cd resonance line in sample 5 using short recovery times $\tau = 1, 2$ s. This ensures that any slow relaxing component is completely saturated and if there are fast relaxing components they should be detected. The measurements were done at room temperature and for different orientations of the crystal. After signal averaging for 20000 and 10000 times respectively no structure in the spectrum could be seen. The resonance line does not depend on the orientation of the crystal in the external magnetic field. A spectrum of ^{113}Cd in sample 5 is shown in figure 4.13 together with a spectrum of ^{113}Cd in sample 1. The data were gained within 24 hours of continuous measurements. The

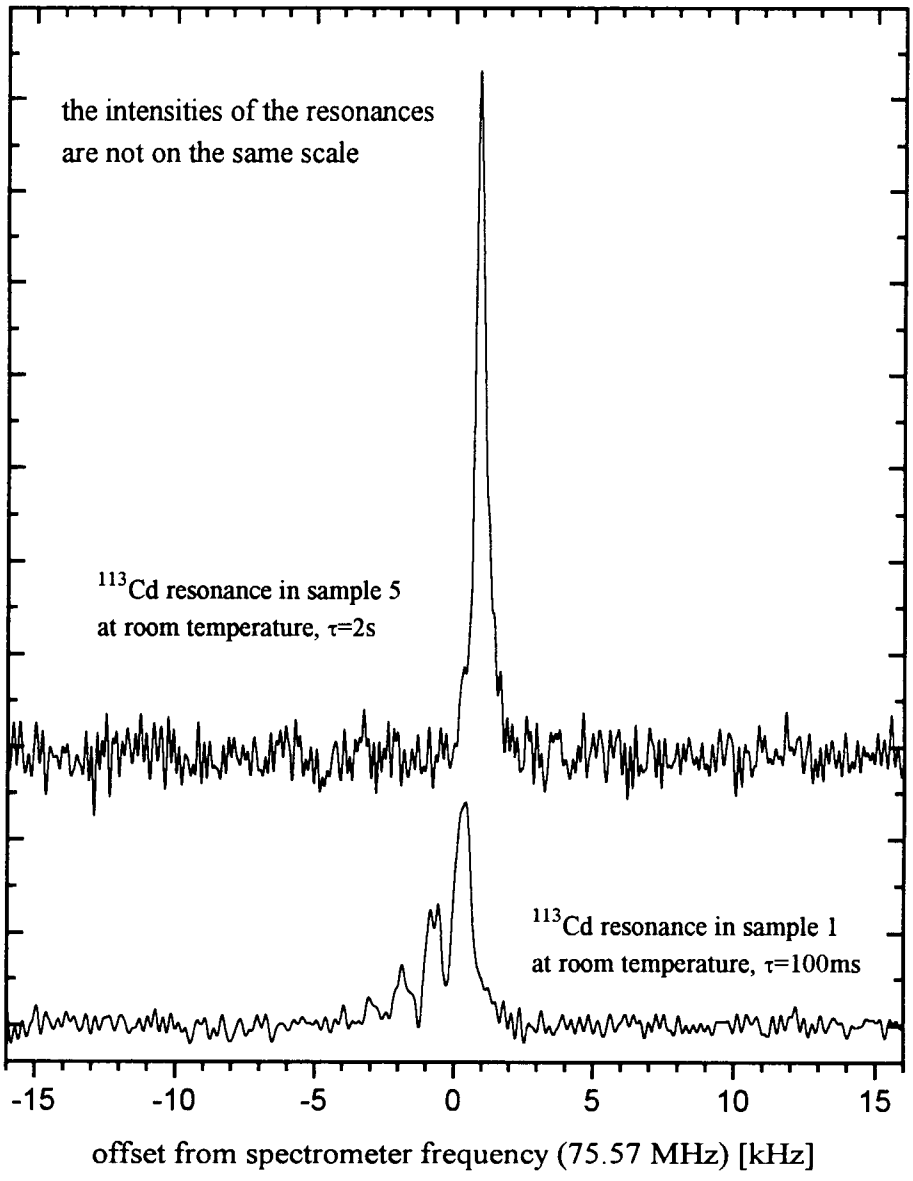

FIG. 4.13. Spectrum of Cadmium in Sample 5

peak	offset [kHz]	line width [kHz]	shift [ppm]
sample 5 peak 0	0.92 ± 0.03	0.47 ± 0.03	276 ± 2
sample 1 peak 1	0.34 ± 0.03	0.8 ± 0.1	268 ± 2
sample 1 peak 2	-0.7 ± 0.04	-	255 ± 2
sample 1 peak 3	-1.8 ± 0.1	-	240 ± 3

TABLE VI. Data on ^{113}Cd in Sample 5 and 1

shift of the resonance of cadmium in sample 1 compared to figure 4.9 is explained by the temperature dependence of the chemical shift for ^{113}Cd in cadmium telluride as measured in samples 2, 3 and 4. At higher temperatures the resonance shifts to lower frequencies with a rate of $(-0.12 \pm .02)\frac{\text{ppm}}{\text{K}}$. The temperature difference between the spectra in figure 4.13 and in figure 4.9 is 75 K so that a shift of (9 ± 1.5) ppm i.e. (680 ± 113) Hz occurs. This shift has to be added to the data in table VI if one compares them to previous data (table IV).

The systematic in the shift of ^{113}Cd in indium doped cadmium telluride becomes clear looking at figure 4.13: peak 1 with the longest relaxation time is also shifted the least compared to the reference sample 5 (peak 0). The other peaks behave in the same way i.e. the further they are shifted the shorter is their spin-lattice relaxation time. This effect must be due to the indium dopant in the crystal because it could not be seen in the gallium doped sample nor in an undoped sample.

4.3.7. Discussion

A theoretical expression for the chemical shift of ^{113}Cd in cadmium telluride is given by Willig [26]. The shift is calculated from the band structure and it has a diamagnetic and a paramagnetic contribution. The diamagnetic contribution is

small for ^{113}Cd in CdTe. The paramagnetic part is created by those fundamental and excited electron states which contain appreciably p-like wave functions. A theoretical value of $\delta = 274$ ppm is reported and in very good agreement with the values measured in this work. Willig does not discuss a temperature dependence, but the general expression he uses includes a sum over all electron states in the conduction and valence band where the gap energy is in the denominator. The paramagnetic shift is also proportional to the expectation value $\langle r^{-3} \rangle$ of the electrons in a cubic lattice cell. The change of the gap energy with temperature cannot be used to explain the temperature dependence, since the shift should then be larger at room temperature than at lower temperatures ($E_{gap}(80\ \mathrm{K}) = 1.6$ eV, $E_{gap}(300\ \mathrm{K}) = 1.44$ eV). However the temperature dependence of the expectation value $\langle r^{-3} \rangle$ will change (thermal expansion) and thus the shift should get smaller at higher temperatures. This is in qualitative agreement with my observations. A quantitative analysis would require a detailed band structure calculation at different temperatures and be beyond the scope of this work.

The line width of ^{113}Cd in all samples is larger than it is expected if the line width were due to dipolar broadening only. A small variation of about $(1.5 - 3.5)\%$ in the chemical shift throughout the samples can provide a broadening of this size. The line width of ^{113}Cd in sample 4 (CdTe powder) is larger than the line widths found in single crystals which may be explained as a wider distribution of chemical shifts due to strains in the crystallites introduced in the powdering process. The line width decreases slightly with temperature, which can be explained by the negative temperature gradient of the chemical shift.

It is not clear what causes the high relaxation rate in the undoped powder at high temperatures. This observation seems to be a manifestation of the complex

native defect structure and self-doping effects in cadmium telluride, which are not yet fully understood.

The most apparent result of the measurements of the resonances of ^{113}Cd in all samples is that in case of indium doped samples there are cadmium sites which experience different local fields of a well defined strength and that nuclei on those sites interact with the lattice on a different time scale, i.e. they have different spin-lattice relaxation times T_1. There is a systematic behavior i.e. sites with less paramagnetic shifts relax faster and the intensities are such that the less paramagnetic the shift and the faster the relaxation the fewer sites of that kind exist. In case of sample 1 the intensities of all of those sites compared to the slower relaxing sites are of the order of the fraction of indium nuclei in the sample. This effect could not be seen in the gallium doped sample nor in the undoped samples of cadmium telluride, so that at this point we can only conclude that it is caused either directly by the indium dopant or by the high carrier concentration.

The difference between the two indium doped samples is the different dopant concentration in the two samples. Sample 1 has 15 times more indium nuclei than sample 2, yet it has about the same carrier concentration as sample 2 and the carrier concentrations of both samples 1 and 2 are at least a factor of one hundred higher than in the gallium doped or in the undoped samples. A variation of the free carrier concentration throughout the sample could result in a variation of the spin-lattice relaxation time. At the same time this would result in a variation of Knight shifts, which would have to be distributed in a discrete fashion to explain the data. The Knight shifts have to be shifts to lower magnetic field to explain the data and have indeed been measured by Look and Moore [27]. They report a negative value for the Knight shift in CdTe doped with indium to $10^{18}cm^{-3}$, and a conduction electron density of $9.7 \times 10^{17}cm^{-3}$, and explain the negative Knight

shift by a negative value for the effective g factor g^* of $-(1.1 \pm 0.1)$. They report a value for the Korringa product of $T_1 T K^2 = (g^*)^2 \mu_B^2 / 4\pi\gamma_n^2 \hbar k = (1.6 \pm 0.3) \times 10^{-6}$ Ks and show that the conduction electrons are degenerate at temperatures above 77 K. I have not checked whether the Korringa relation holds for sample 1 or 2 for different temperatures much less whether it holds for the individual peaks. For the spectra shown in figure 4.13 however one can check whether it yields the same order of magnitude. The shift between peak 0 (no Knight shift, undoped sample) and peak 1 is (8 ± 2) ppm at a temperature $T = 300$ K and thus a Korringa product of $(0.8 \pm 0.4) \times 10^{-6}$ Ks can be calculated. The spin-lattice relaxation time $T_1 = (38 \pm 5)$ s at room temperature has been used for the Korringa product but the real value of T_1 is certainly longer, since I have not acquired enough data on the baseline of figure 4.8. Thus the results are in qualitative agreement with a diamagnetic Knight shift. The resonance lines which are shifted to even lower magnetic fields may be due to a locally higher conduction electron density. This variation in conduction electron density throughout the sample might be due to an inhomogeneous distribution of indium dopants in the sample or it might be due to a higher density of states of conduction electrons around the impurity.

Dipole-dipole interactions between the tellurium and the cadmium and also between the indium dopants and the cadmium nuclei will cause shifts in the resonance frequencies. Those shifts should cause a line broadening rather than a discrete shift and their size was estimated to be 200 Hz at most. Line widths of up to 1 kHz were measured, but this is not enough to explain the shifts of 1 to 5 kHz. Different occupations of those sites closest to the cadmium by tellurium and indium would result in different shifts. Since all the measurements were done at temperatures at which kT is larger than the energy quanta required for a spin flip, i.e. the nuclei obey the Boltzmann distribution, it is clear that shifts due to dipole-dipole inter-

actions have to be symmetric with respect to a non-shifted line. The data do not match this requirement.

5. CONCLUSION

5.1. SUMMARY

This work describes NMR measurements in different samples of doped and undoped cadmium telluride. The dopants are gallium and indium of group III of the periodic table. They replace cadmium in the zinc blende lattice. In order to investigate orientational dependencies of hyperfine interactions experienced by the nuclei the measurements were done on single crystals. Since the samples are doped to high concentrations $(1.0 - 15) \times 10^{19}\text{cm}^{-3}$ the skin effect excluded the use of echo sequences involving a π-pulse (see figure 3.4). Therefore in almost all of the measurements a saturation sequence was used, which also allowed higher repetition rates.

I was not able to attribute a definite signal to indium in sample 1 or 2. This is surprising if one analyses the PAC data on indium doped CdTe and estimates the quadrupole shift of indium expected for NMR measurements. A possible explanation is the huge difference in sensitivity of the two methods. PAC can be observed in the presence of large electric field gradients, but it can not pick up small variations i.e. distributions in those gradients. NMR is very sensitive even to very small electric field gradients. Thus a distribution in field gradients can broaden the line to an extent where the intensity is too small to be detected. This gets aggravated by the fact that I am looking at a dilute solution of spins which inherently has a small intensity.

Gallium resonances were found in sample 3. The dominant relaxation process of gallium in CdTe is quadrupolar relaxation, i.e. the coupling of the quadrupole

moment of both gallium isotopes to the electric field gradients which vary in time caused by phonons. There are three different environments experienced by the gallium nuclei in CdTe. One part sits on lattice sites without static field gradients. Another fraction experiences a small field gradient with a coupling constant of about 3.5 kHz. Of another part of the nuclei it is clear that they experience a field gradient, but whether it is a distribution of gradients or not remains to be seen.

NMR measurements on cadmium are relatively easy to do because it is a host species and because ^{113}Cd has spin one half and high abundance. The magnetic shift of the resonance line in sample 3 and 4 has a negative temperature gradient. The shift is here defined as $\delta = (\nu_{sample} - \nu_{reference})/\nu_{reference}$ and a 0.1 molar solution of $CdSO_4$ was used as a reference [20]. The temperature dependence is in qualitative agreement with a theoretical expression for the chemical shift in CdTe given by Willig [26].

The spin-lattice relaxation time T_1 in sample 3 (doped with gallium to 10^{19}cm^{-3}) is (500 ± 10) s and the line width is 370 Hz at room temperature. In sample 4 (undoped CdTe powder) a T_1 of (583 ± 23) s at $T = 273$ K and a line width of 1100 Hz is found.

In sample 2 (doped with indium to 10^{19}cm^{-3}) a T_1 of (11 ± 4) s at $T = 223$ K is found, while $T_1 = (38 \pm 5)$ s in sample 1 (doped with indium to 1.5×10^{20}cm^{-3}) is longer. The much shorter T_1 is expected since the concentration of free carriers is by 2 orders of magnitude higher than in sample 3. However sample 3 exhibits a Korringa like temperature dependence of the spin-lattice relaxation time, i.e. as if the relaxation is due to degenerate conduction electrons. Sample 4 does not have a feature like this but its relaxation rate actually increases with higher temperatures to values higher than those found in sample 3. An explanation for this is not yet known.

Very fast relaxing cadmium sites are found in sample 1 and 2. Up to five distinct lines shifted to lower frequencies are found. The splitting between the lines is about (13 ± 3) ppm and the line widths are approximately (0.9 ± 0.1) kHz. The further the resonances are shifted the faster is their relaxation time and the lower is their intensity. The total fraction of cadmium resonances shifted in frequency is of the order of the indium concentration in the sample. The splitting does not depend on the orientation of the crystal in the external field and also does not depend on temperature, at least within $T = 223 - 300$ K. Whether it depends on the magnitude of the external field is not known. So far I do not have an explanation for the observed behavior.

5.2. SUGGESTIONS FOR FURTHER RESEARCH

The NMR measurements done in this work have shown that NMR is an effective method to directly gather data on the microscopic environment of dopants in CdTe. Data on the effects of doping in cadmium telluride can be gained by NMR on ^{113}Cd, the host nuclei.

NMR on highly doped single crystals is time consuming since the skin effect partly shields the sample from the radiofrequency field used to do the measurement. To get information on the host nuclei which do not experience quadrupole interactions a powder sample might be more efficient, but the effect of the powdering process must be carefully investigated (line broadening due to induced strains).

In the gallium doped sample 3 it would be interesting to see whether the sharp echo in the time domain corresponds to just a broad line in frequency space or whether it has some structure. This experiment would need a higher resolution in

time domain so that a structure can be resolved. One can then alter the spectrometer frequency step by step.

The indium doped crystals are very interesting since the concentration of free carriers is larger than in the gallium doped sample. This results in a shorter T_1 for the host nuclei. It will be interesting to determine the origin of the distinct Cd sites in sample 1 and 2. This would be assisted by a precise measurement of the individual T_1 relaxation times for the different sites. Samples doped to different and lower concentrations would allow one to measure in which way this effect depends on concentration. An exact measurement of the ratio of the intensities of the fast relaxing nuclei to the intensity of the slower relaxing nuclei in samples of different indium concentration would help to decide whether the effect is a direct indium cadmium interaction or whether it is primarily caused by the higher free carrier concentration in the indium doped samples. Highly reliable Hall data are needed at the same time. Measuring the distinct sites before and after an annealing treatment together with precise Hall data before and after the annealing should provide valuable information on the nature and on the dynamics of the defects causing the splitting.

BIBLIOGRAPHY

[1] K. Zanio, *Semiconductors and Semimetals, vol.13, Cadmium Telluride*, Academic Press, New York, 1978

[2] T. Wichert, T. Krings, H. Wolf, "Characterization of ZnSe and other II-VI semiconductors by radioactive dopants", Physica B, **185**, 297-307, (1993)

[3] H. Hartmann, R. Mach, B. Selle, *"Wide Gap II-VI Compounds as Electronic Materials"* in Current Topics in Material Science, E. Kaldis editor, North-Holland Publishing Company, Amsterdam, Vol.9, 1982

[4] G. L. Hansen et. al., "Energy gap versus alloy composition and temperature in $Hg_{1-x}Cd_xTe$", J. Appl. Phys., **53**, 7099-7101, (1982)

[5] M. Aven, J. S. Prenner editors, *Physics and Chemistry of II-VI Compounds*, North-Holland Publishing Company, Amsterdam, 1967

[6] E. Watson, D. Shaw, "The solubility and diffusivity of In in CdTe", J. Phys. C: Solid State Physics, **16**, 515-37, (1983)

[7] N. C. Giles et. al., "The effects of a high-temperature anneal on the electrical and optical properties of bulk CdTe:In", J. Appl. Phys., **64**, 2656-65, (1988)

[8] G. W. Blackmore et. al., "Diffusion of gallium in cadmium telluride.", Materials Science and Engineering, **B16**, 186-190, (1993)

[9] D. Wegner, E. A. Meyer, "Evidence of In-defect complexes in CdTe", J. Phys.: Condens. Matter, **1**, 5403-10, (1989)

[10] R. Kalish, M. Deicher, G. Schatz, "Annealing of indium-implanted CdTe", J. Appl. Phys., **53**, 4793-4799, (1982)

[11] J. W. Griffith, R. Lundquist, R. Platzer, J. A. Gardner, "Indium Donor Complexes with Vacancies in CdTe and ZnSe", *Defects in Semiconductors 17*, Proceedings of the seventeenth international conference, to be published

[12] C. P. Slichter, *Principles of Magnetic Resonance*, third edition, Springer, Berlin Heidelberg New York, 1990

[13] M. Mehring, *Principles of High-Resolution NMR in Solids*, second edition, Springer, Berlin Heidelberg New York, 1983

[14] M. H. Cohen and F. Reif, *Quadrupole Effects in Nuclear Magnetic Resonance Studies of Solids* in Solid State Physics, Volume 5, p. 321 ff., F. Seitz, D. Turnbull editors, Academic Press, Inc., New York, 1957

[15] J. D. Jackson , *Classical Electrodynamics*, second edition, John Wiley & Sons, New York, 1975

[16] A. Abragam, *Principles of Nuclear Magnetism*, Clarendon Press, Oxford, 1961

[17] B. C. Gerstein, C. R. Dybowski, *Transient Techniques in NMR of Solids,* Academic Press, New York, 1985

[18] G. H. Stauss, "Nuclear Magnetic Resonance Determination of Some Microscopic Parameters of $LiAl_5O_8$", J. Chem. Phys., **40**, 1988-91, (1964)

[19] T. P. Das, P. C. Schmidt, "Current Status of Theory of Nuclear Quadrupole Interaction in Metallic Systems", Z. Naturforsch., **41**a, 47-77, (1986)

[20] R. J. Kostelnik, A. A. Bothner-By, "Cadmium-113 Nuclear Magnetic Resonance Studies of Cadmium(II)-Ligand Binding in Aqueous Solutions. I. The Effect of Diverse Ligands on the Cadmium-113 Chemical Shift", J. Magn. Res., **14**, 141-151, (1974)

[21] R. L. Mieher, "Quadrupolar Nuclear Relaxation in the III-V Compounds", Phys. Rev., **125**, 1537-51, (1962)

[22] D. Freude, J. Haase, *Quadrupole Effects in Solid-State Nuclear Magnetic Resonance*, NMR Basic Principles and Progress, Springer, in press

[23] N. W. Ashcroft, N. D. Mermin, *Solid State Physics*, Saunders College, Philadelphia, 1976

[24] N. Bloembergen, "Nuclear Magnetic Relaxation in Semiconductors", Physica, **20**, 1130-33, (1949)

[25] W. W. Warren, R. E. Norberg, "Multiple-Pulse Nuclear-Magnetic-Resonance Transients of ^{129}Xe and ^{131}Xe in Solid Xenon", Phys. Rev., **154**, 277-86, (1967)

[26] A. Willig, B. Sapoval, K. Leibler, C. Vérié, "Chemical Shift of NMR in HgTe, CdTe and their Alloys", J. Phys. C: Solid State Phys., **9**, 1981-89, (1976)

[27] D. C. Look, D. L. Moore, "Nuclear-Magnetic-Resonance Measurement of the Conduction-Electron g Factor in CdTe", Phys. Rev. B, **5**, 3406-3412, (1972)